FACULTY OF TECHNOLOGY

STUDYING THE IMPACT OF HYDRODYNAMIC CONDITIONS ON THE FLOTATION PERFORMANCE OF A PORPHYRY COPPER

Byeryekgul Myezimkhan

DEGREE PROGRAMME

Master’s thesis

June 2024

CONSTANCIA DE VALIDACIÓN Y CONFIDENCIALIDAD DE MONOGRAFÍA A REPOSITORIO ACADÉMICO

1.- IDENTIFICACIÓN DEL TRABAJO ACADÉMICO

Tipo de monografía (marcar una opción): ☐ Memoria o trabajo de título; ☒ Tesis de Postgrado;

Título del trabajo: Studying the impact of hydrodynamic conditions on the flotation performance of a porphyry copepr

Nombre del candidato(a): Byeryekgul Myezimkhan

Carrera / Grado: Master of Science

Campus: Casa Central Valparaiso ; **Departamento**: Chemical and Environmental Engineering

2.- VALIDACIÓN DEL PROFESOR GUÍA/DIRECTOR DE TESIS

Yo, , en mi calidad de profesor(a) guía/director(a) del trabajo académico mencionado anteriormente **DEJO CONSTANCIA** que:

- He revisado esta versión del documento y corresponde a la versión final aprobada del trabajo.
- El trabajo cumple con los requisitos académicos y de formato establecidos por la institución

3.- EVALUACIÓN DE CONFIDENCIALIDAD POR PROPIEDAD INDUSTRIAL

☒ El trabajo **NO contiene información que amerite confidencialidad** y puede ser publicado de inmediato en repositorio con acceso abierto.

☐ El trabajo **CONTIENE** información con potenciales implicancias de propiedad industrial o intelectual y requiere un periodo de confidencialidad (embargo) por:

☐ 6 meses; ☐ 12 meses; ☐ 2 años; ☐ 3 años; ☐ 5 años; ☐ 10 años

Fundamentación de la necesidad de confidencialidad (obligatorio si se solicita embargo):

4.- FIRMAS

Profesor(a) guía o director(a) de memoria o tesis:

LUIS EDUARDO VINNETT PERALTA

Digitally signed by LUIS EDUARDO VINNETT PERALTA
Date: 2025.10.12 20:18:16 -03'00'

Fecha: ; **Firma:** _____

Estudiante o Candidato(a):

Fecha: 07/10/2025 ; **Firma:** _____

Este formulario debe ser insertado como página 2 de la memoria o tesis, completado y firmado por estudiante y profesor(a) antes de la entrega en portal PRISMA de Biblioteca USM.

STUDYING THE IMPACT OF HYDRODYNAMIC CONDITIONS ON THE FLOTATION PERFORMANCE OF A PORPHYRY COPPER ORE

Byeryekgul Myezimkhan

DEGREE PROGRAMME

Master's thesis

June 2024

FACULTY OF TECHNOLOGY, OULU MINING SCHOOL, UO

DEPARTMENT MINERAL RESOURCES ENGINEERING, CHAIR OF MINERAL PROCESSING, MUL

FACULTY OF MINING, GEOLOGY AND PETROLEUM ENGINEERING, UNIZG

DEPARTMENT OF CHEMICAL AND ENVIRONMENTAL ENGINEERING, UTFSM

STUDYING THE IMPACT OF HYDRODYNAMIC CONDITIONS ON THE FLOTATION PERFORMANCE OF A PORPHYRY COPPER

Byeryekgul Myezimkhan

DEGREE PROGRAMME EMJM-PROMISE

Erasmus Mundus Joint Master in Sustainable Mineral and Metal Processing Engineering

June 2024

ABSTRACT

Studying the Impact of Hydrodynamic Conditions on the Flotation Performance of a Porphyry Copper

Byeryekgul Myezimkhan

University of Oulu, Erasmus Mundus Joint Master in Sustainable Mineral and Metal Processing Engineering

Master's thesis, 2024, 62 pp. 8 pp. appendixes

Supervisor at the university: Prof. Luis Vinnett

Co-supervisor: Prof. Claudio Acuña-Perez

Co-supervisors at host institution: Dr. Lucas Pereira, Dr. Martin Rudolph, Ali Hassan

The thesis investigates the influence of hydrodynamic conditions on the batch flotation performance of a porphyry copper ore, utilizing 6-liter and 35-liter cells. The main objective is to determine the effects of variations in impeller tip speed (V_t) and superficial gas velocity (J_g) on performance indices such as recovery, grade, and rate constant.

Flotation tests were conducted at the studied scales varying V_t and J_g. Factors influencing flotation performance were identified by regression analysis. In addition, particle-based separation modeling (PSM) was conducted, using Mineral Liberation Analyzer (MLA) data to provide detailed insights into the flotation of particles with different characteristics. This modeling method enabled a comprehensive understanding of how particle size, shape, surface composition, and mineral content affected flotation performance.

The results indicated that in the 35-liter cell, both V_t and J_g significantly impacted the flotation recovery, with V_t having a positive effect and J_g a negative effect. In the 6-liter cell, neither V_t nor J_g significantly influenced the performance indices. A comparison between portable X-ray fluorescence (pXRF) and MLA results for the 6-liter cell tests showed consistent trends, confirming the reliability of the analysis techniques, which

made it possible to use only pXRF in the 35-liter cell tests. The main findings suggested that an adequate selection of V_t and J_g allows for the optimization of flotation performance. This research provides a foundation for future studies aimed at improving flotation of porphyry copper ores, offering valuable insights for both academic research and practical applications in mineral processing.

Keywords: flotation, hydrodynamics, impeller tip speed, superficial gas velocity, particle-based separation modeling

FOREWORD

I would like to express my deepest gratitude to my academic supervisor, Professor Luis Vinnett, for his unwavering support and profound belief in my work. I am also extremely grateful to my co-supervisors, Dr. Lucas Pereira, Dr. Martin Rudolph, and Ali Hassan, for their extensive knowledge, valuable contributions, and patience throughout my thesis project. The completion of this work would not have been possible without their guidance and support.

I extend my sincere appreciation to all professors and lecturers at Universidad Técnica Federico Santa María, Montanuniversität Leoben, and the University of Oulu, who have guided me throughout my master's study. Furthermore, I am grateful to the processing department of the Helmholtz Institute Freiberg for Resource Technology (HIF) for their constant support, and provision of necessary resources and facilities. Particularly, I would like to thank Rocco Naumann, Kai Bachmann, Joachim Krause, Roland Würkert, and Doreen Ebert for their contributions to my experimental work. I also extend my thanks to Renate Seidel and Sandra Birtel for their vital administrative work in keeping the wheels turning smoothly.

Finally, I would like to convey my heartfelt appreciation to my family and friends for their unwavering support and encouragement, which has been instrumental in helping me overcome the challenges encountered throughout this journey.

Oulu, 14.06.2024

Byeryekgul Myezimkhan
Byeryekgul Myezimkhan

TABLE OF CONTENTS

ABSTRACT
FOREWORDS
TABLE OF CONTENTS
LIST OF ABBREVIATIONS
1 Introduction 1
1.1 General objective 4
2 Literature review 6
2.1 Fundamentals of froth flotation 6
2.2 Hydrodynamics of particle-bubble interaction 10
2.3 Key factors influencing hydrodynamics in flotation 13
2.4 Flotation reagents 16
2.5 Flotation kinetics 19
2.6 Rate constant as a function of a process variable 20
2.7 Particle-based modeling in flotation 22
3 Research process 24
3.1 Material 24
3.2 Experiments 25
3.3 Analytic techniques 30
4 Assessment of the results 34
4.1 6-liter flotation tests: regression analysis 34
4.2 35-liter flotation tests: regression analysis 35
4.3 Analyzing scale variations: hydrodynamics in the 6-liter and 35-liter flotation cells 38
4.4 Comparative analysis of pXRF and MLA results 38
4.5 Particle-based separation modeling 40
5 Conclusions and Recommendations 51
6 Summary 53
REFERENCES 55
APPENDICES:
Appendix 1. Residuals plot for regression analysis results of 6-liter flotation test.
Appendix 2. Results of experimental design at 5 g/t of collector dosage.

LIST OF ABBREVIATIONS

J_g	superficial gas velocity
V_t	impeller tip speed
k	rate constant
ECD	equivalent circle diameter
DoE	design of experiment
MLA	mineral liberation analyzer
pXRF	portable X-ray fluorescence
PSM	particle-based separation model
HIF	Helmholtz Institute Freiberg for Resources and Technology

1 INTRODUCTION

Copper (Cu) is a critical element underpinning various sectors crucial to modern society, including construction, power, and information technology. Its importance in driving global economic growth and enabling the transition to a low-carbon future cannot be overstated (Valenta et al., 2019). The achievement of many United Nations Sustainable Development Goals (SDGs), from health and well-being to clean water and sanitation, is contingent upon the continued supply of Cu (The Role of Critical Minerals in Clean Energy Transitions, 2021). However, the Cu mining industry is facing significant challenges, as high-grade ores are being depleted and more complex deposits need to be processed.

To illustrate this issue, Figure 1 shows the historical decline in copper ore grades for reserves and/or resources in selected countries, including Australia, Papua New Guinea (PNG), Poland, India, and the United States. This figure highlights a notable change in the average copper grade for Australia, which is likely attributed to the incorporation of high-grade deposits such as Mount Isa or Olympic Dam. These data demonstrate an overall long-term decline in the Cu grades of mineral resources over time. This trend is expected to continue, with world average grades to fall below 0.5% (Mudd & Jowitt, 2018).

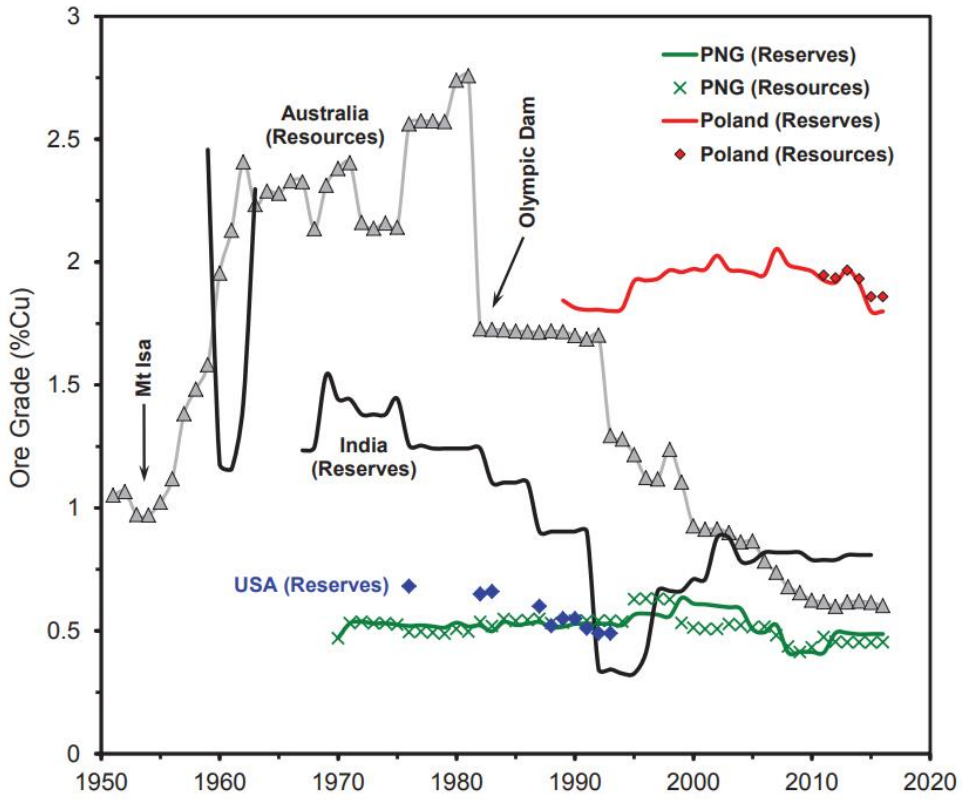

Figure 1. Historical historical data on the ore grades of reserves and/or resources for selected countries, namely Australia, PNG, Poland, India, and the United States. Modified from Mudd & Jowitt (2018).

As ore grades decline, beneficiation plants are subject to critical constraints. These include the need for increases in throughput, fine grinding to obtain targeted levels of liberation, the presence of ultrafine particles, higher energy consumption, among others (Wills & Finch, 2016). Thus, to effectively and selectively separate valuable minerals, mining and mineral processing industries require highly efficient processes, along with new technologies for concentration and ore characterization.

Froth flotation is the most widely used physico-chemical separation method in the mining industry. It processes over two billion tonnes of primary and secondary resources annually (Hassanzadeh et al., 2022), representing approximately 15% of world mining production (Christian & Michael, 2023). In this process, valuable minerals are selectively separated from gangue minerals. However, a significant fraction of valuable minerals is lost in the tailings as both fine and coarse particles.

Recovery (R) as a function of particle size (d_p) typically follows the concave trend depicted in Figure 2. Optimum recoveries are obtained in intermediate sizes, while recovery decreases for very fine and very coarse particles (Trahar, 1981). Low recoveries in the fine size classes are commonly attributed to low probability of particle-bubble collision, whereas low recoveries in the coarse size classes are mainly attributed to high probability of particle-bubble detachment or poor liberation (Wills & Finch, 2016).

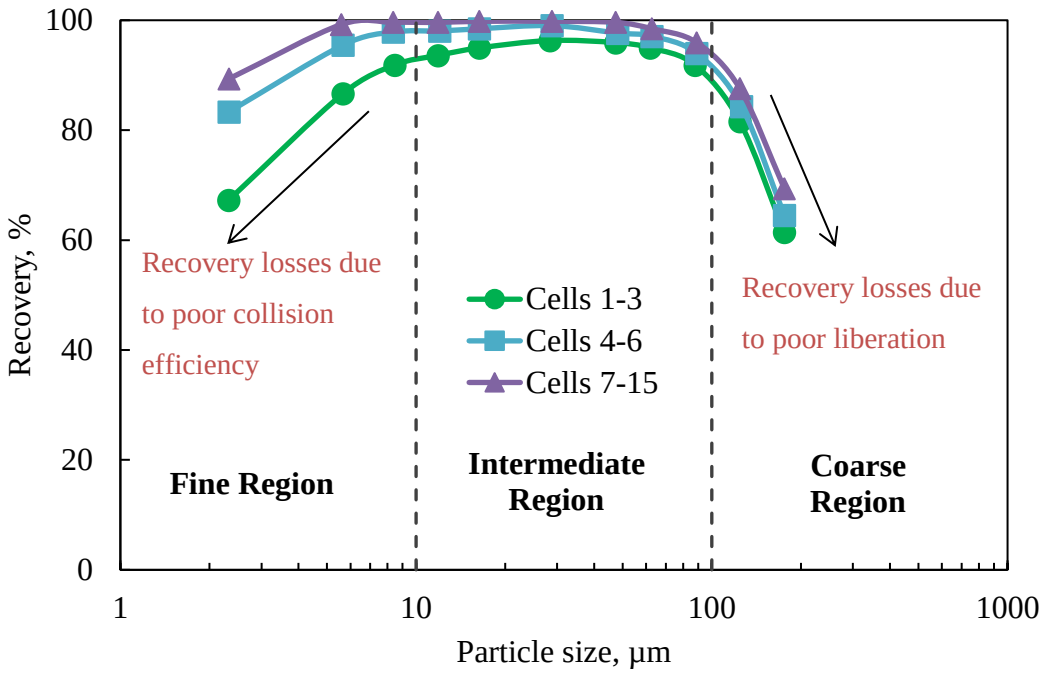

Figure 2. Recovery as a function of particle size. Modified from Trahar (1981).

Figure 3 shows the interactions between fine and coarse particles and a bubble in a flotation machine. Fine particles tend to remain suspended in the slurry, whereas coarse particles tend to settle to the bottom of the cell. The intermediate-sized particles are more prone to succesfully collide with and attach to the rising bubbles, leading to higher recoveries. An adequate adjustment of the hydrodynamic conditions in a flotation cell, such as impeller speed and air flow rate, may enhance the recovery of difficult-to-float particles by promoting collision and adhesion efficiencies (Kawatra & Young, 2019).

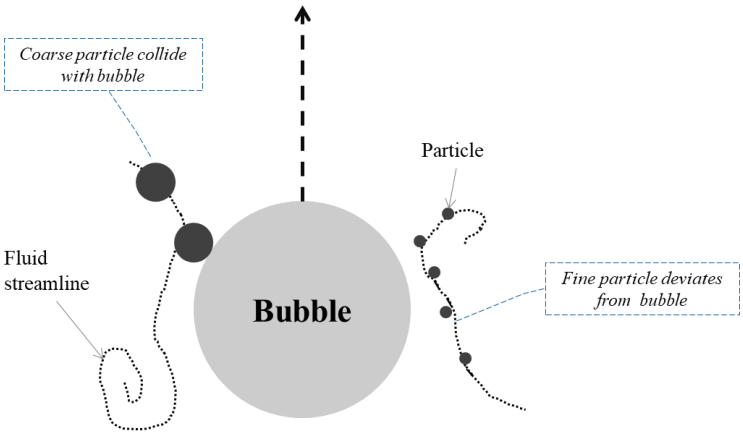

Figure 3. Interactions between fine and coarse particles and a bubble in a flotation machine.

This master's thesis aims to study the relationship between hydrodynamic conditions and flotation performance, specifically focusing on the batch flotation of a porphyry copper ore. Experiments were conducted in 6-liter and 35-liter flotation cells, which incorporated the FLSmidth nextSTEP rotor/stator system. Analytical techniques such as portable X-ray fluorescence (pXRF) and Mineral Liberation Analyzer (MLA) were employed for metallurgical assessment and mineralogical characterization, respectively. The mineralogical features were related to the flotation performance for a better understanding on how machine hydrodynamics and scales influence the separation of individual particles at batch scale.

1.1 General objective

The main objective of the master's thesis was:

To investigate the impact of different machine scales (6-liter and 35-liter) and hydrodynamic conditions on the batch separation of a porphyry copper ore, using the FLSmidth nextSTEP rotor/stator system.

The specific objectives were:

- To study the influence of the impeller tip speed and superficial gas velocity on the flotation performance of a 6-liter cell.
- To analyze differences in the flotation results when separating the copper ore in 6-liter and 35-liter flotation cells.
- To study mineral composition and liberation, using MLA, on selected samples.
- To integrate the hydrodynamic and mineralogical findings to improve the beneficiation of the porphyry copper ore.
- To use particle-based separation modeling for a better understanding of the flotation performance of individual particles.

This thesis is organized as follows: Chapter 2 presents a literature review on flotation fundamentals and hydrodynamics; Chapter 3 describes the experimental methodology; The results are presented in Chapter 4; and the main conclusions and recommendations are summarized in Chapter 5.

2 LITERATURE REVIEW

2.1 Fundamentals of froth flotation

The primary objective of mineral processing is to concentrate valuable minerals out of gangue minerals. Flotation employs differences in the surface properties of the minerals in the concentration process. These surface properties are modified into hydrophobic or hydrophilic states via chemical reagents. The effectiveness of the separation also depends on the interaction between hydrophobic particles and air bubbles: collision, adhesion, and aggregate transport to the top of the machine (Wills & Finch, 2016). The buoyant forces allow the particle-bubble aggregates to ascend, forming a froth phase at the top. This froth is discharged as an enriched product, referred as a concentrate. Hydrophilic particles that do not adhere to the bubbles remain suspended in the pulp and are subsequently rejected in the tailings. This selective separation allows for the concentration of minerals and their recovery. Low-grade and complex ores containing valuable minerals can efficiently be treated by froth flotation.

The flotation process is a rather complex system, involving three phases (solid, liquid, and gas/air), as well as physical and chemical variables. Physical variables within this system include ore-related properties (particle size, shape, mineral composition), and machine-derived factors such as air flowrate, bubble size, and froth depth. Chemical variables govern surface interactions. A schematic of the process is depicted in Figure 4. In this setup, the pulp/slurry contains suspended particles, water, chemical reagents, and air bubbles. This pulp is agitated by an impeller, a mechanical device that stirs the mixture. The generation of air bubbles at the bottom of the flotation cell favors the formation of the froth layer at the top of the machine. This froth layer, mostly containing hydrophobic particles, is then overflowed as an enriched product.

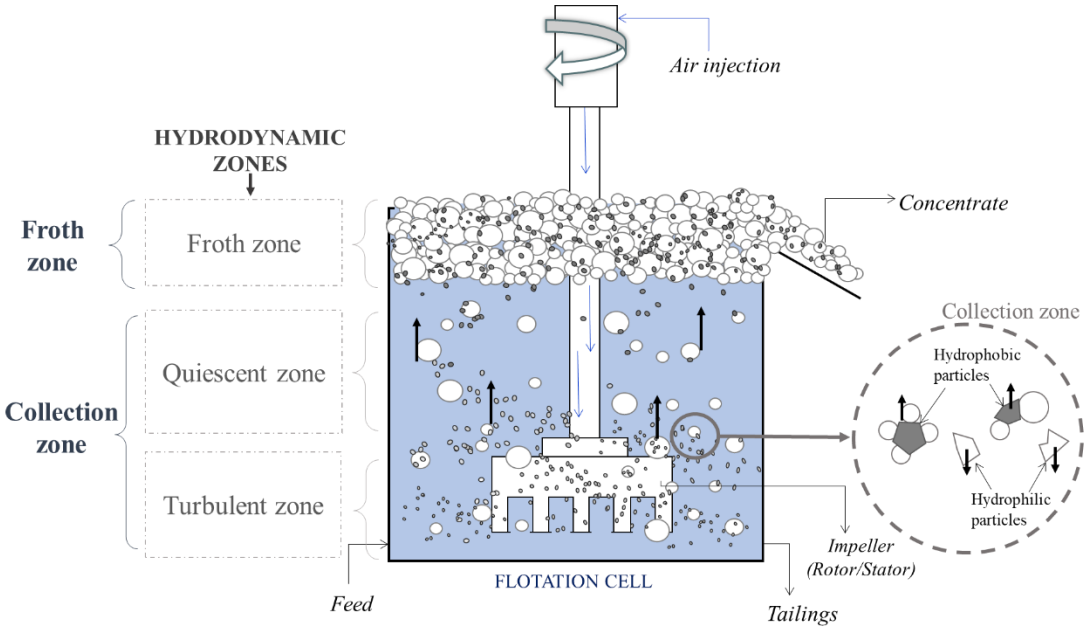

Figure 4. Hydrodynamic regions and its components within a flotation cell. Modified from Wills & Finch (2016).

The flotation cell is typically divided into two distinct zones: the collection zone (or pulp zone), where the particle-bubble aggregates are formed, and the froth zone, where the flotation product is enriched (Hu et al., 2003; Vinnett et al., 2012; Wills & Finch, 2016). Efficient particle collection in the pulp zone is mainly influenced by hydrodynamic conditions and operational parameters such as airflow rate, impeller tip speed, and solid content.

Turbulence is necessary in the collection zone to promote the interactions between the particles and the bubbles (Schubert & Bischofberger, 1978). The collection zone is subdivided into two subzones based on the turbulence intensity:

- Turbulent zone, where the injected air is dispersed into bubbles, and particle-bubble interaction occurs, allowing minerals to be collected on the bubble surface. Around the rotor region, the local energy dissipation is significantly greater than the mean energy dissipation (Schubert, 1999).

- Quiescent zone, located above the turbulent region, where the turbulence intensity is significantly lower. Within this calm zone, particle-bubble aggregates rise to the froth phase (Wills & Finch, 2016).

The froth zone is as a cleaning stage that eliminates hydrophilic particles and middlings carried along with water streamlines (entrainment). This particle rejection is indicated by the drop-back stream in Figure 5, which enhances the process selectivity. The particles that are not drained out from the froth zone are recovered into the concentrate stream.

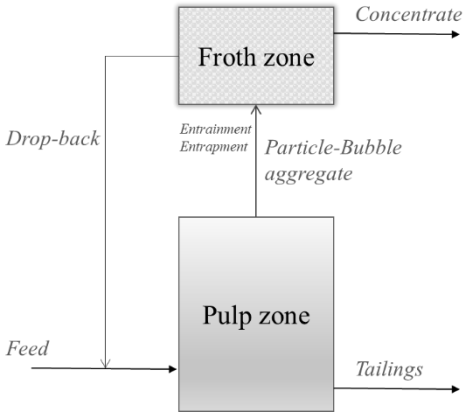

Figure 5. Schematic of the two interacting zones in flotation: pulp and froth. Modified from Wills & Finch (2016).

The overall flotation efficiency is influenced by several internal factors, including particle size distribution (PSD), mineral liberation, pulp density and viscosity, bubble size distribution (BSD), chemical environment, turbulence, froth stability, among others. From a macroscopic perspective, the efficiency of a flotation process is quantified by the mineral or metal recovery, *R*, which refers to the flow or mass of a component in the concentrate regarding the flow or mass of the same component in the feed. Equation (1) expresses the recovery of a mineral or metal in a flotation system (Wills & Finch, 2016).

$$R = \frac{c\,C}{f\,F}\,100,\ \%\qquad(1)$$

Within Equation (1):

c is the grade of the mineral/metal in the concentrate,

C is the concentrate flow rate,

f is the grade of the mineral/metal in the feed, and

F is the feed flow rate.

Particles are recovered in flotation by three mechanisms: true flotation, entrainment, and entrapment (Wills & Finch, 2016). True flotation exploits variations in surface properties among mineral particles; hydrophobic minerals form stable aggregates with bubbles (so-called particle-bubble aggregates), which buoys to the top of the machine. The flotation process exhibits random features; consequently, probabilistic instead of deterministic events are more representative of the sequential stages in the separation system. These events involve collision, adhesion, and stability, as described by Gaudin (1932), and expressed as probabilities by Schuhmann (1942). Figure 6 illustrates the sequence of events to obtain the particle-bubble aggregate.

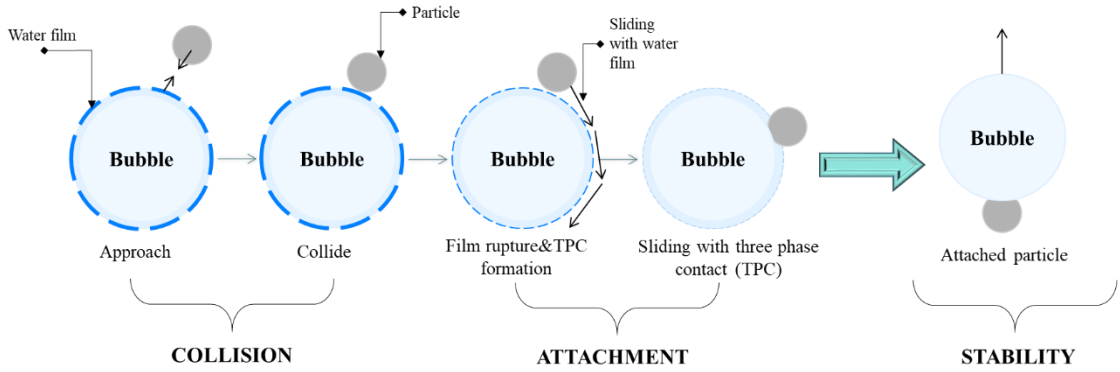

Figure 6. Schematic of particle and bubble interactions in a flotation machine. Modified from Wang et al. (2020).

Each stage in this process depends on the particle-bubble interactions, which can be manipulated, if necessary, changing the hydrodynamic conditions. Thus, understanding flotation hydrodynamics and mineral properties is critical for a succesful separation.

2.2 Hydrodynamics of particle-bubble interaction

Successful interaction between particles and bubbles in flotation processes occurs when the pulp is properly, making the particles more prone to interacting with bubbles (Ahmed & Jameson, 1989). The probability of the particle-bubble collection can be mathematically expressed by equation (2) (Duan et al., 2003; Yoon, 1993, 2000):

$$P_{coll} = P_c\, P_a\, (1 - P_d) \tag{2}$$

where P_{coll} is the collection probability,
P_c is the probability of particle-bubble collision,
P_d is the probability of particle detachment, and
P_a is the probability of particle-bubble adhesion.

2.2.1 Collision probability

The collision probability between particles and bubbles has been investigated theoretically and experimentally since the late 1960s (e.g., Flint & Howarth, 1971; Reay & Ratcliff, 1973, 1975; Anfruns & Kitchener, 1977; Schulze, 1984; Weber, 1981; Weber & Paddock, 1983; Dobby & Finch, 1987; Yoon & Luttrell, 1989). This probability is highly dependent on the system hydrodynamics, and particle and bubble sizes. Estimating P_c requires multiple factors to be taken into consideration in the evaluation of different analytical models, in which a variety of assumptions has been used in literature (Dai et al., 2000). These models simplify the estimation of collision efficiency by defining fluid regimes (including potential, stoke, and intermediate flows), effective forces (interceptional, gravitational, and inertial), bubble features (size, velocity, surface mobility), particle characteristics (size, density, trajectory), energy dissipation rates, and turbulence intensity (Dai et al., 2000).

Studies conducted by Sutherland (1948) and Gaudin (1957) established the foundation for stream function-based models, which describe the flow patterns around bubbles and particles. These models have been considered applicable to extreme bubble sizes (both excessively large and small bubbles). Subsequent research efforts further refined these models to predict collision probabilities for bubbles sizes typically observed in flotation

(Yoon, 2000). However, the applicability of stream function-based models tends to be poor under conditions of intense agitation, as those commonly observed in industrial flotation machines.

Turbulence models may be more suitable for mechanically agitated cells. According to the model developed by Abrahamson (1975) and Schubert & Bischofberger (1978), the number of particle-bubble collisions per unit volume of slurry and time can be predicted by equation (3).

$$Z_{pb} = 5\, N_p\, N_b \left(\frac{d_p + d_b}{2}\right)^2 \sqrt{\overline{v_p^2} + \overline{v_b^2}}\ , \tag{3}$$

where Z_{pb} is the number of particle-bubble collisions per unit volume of slurry and time,

N_p is the number of particles per unit volume,

N_b is the number of bubbles per unit volume,

d_p is the particle diameter,

d_b is the bubble diameter,

v_p is the mean relative velocities of the particles, and

v_b is the mean relative velocities of the bubbles.

2.2.2 Adhesion probability

Following the particle-bubble collision, the particle may slide over the bubble surface, allowing the attachment (Sutherland, 1948). For successful adhesion, the induction time must be shorter than the sliding time (Dai et al., 2000). The probability of adhesion, as expressed by equation (4) (Nguyen & Schulze, 2003), depends on both the induction time (t_{ind}) and the sliding time (t_c).

$$P_a = 1 - \exp\left(-\frac{t_c}{t_{ind}}\right), \tag{4}$$

Within Equation (4):

t_c is the contact time, and

t_{ind} is the sliding time.

Nguyen & Schulze (2003) proposed a modified Dobby-Finch's model (Finch & Dobby, 1991) to estimate the adhesion probability, as expressed by equation (5):

$$P_a = \sin^2\left(\frac{\theta}{2}\right) \exp\left(-\frac{t_{ind}}{t_c}\right), \tag{5}$$

where θ is the contact angle.

Smaller particles, and those with higher contact angles, exhibit shorter induction times, leading to higher adhesion probabilities (Dai et al., 2000). Smaller bubbles are more likely to attach to particles after collision due to their thinner hydrated layer and larger contact angles (Wang & Liu, 2021).

2.2.3 Detachment probability

Turbulence and gravitational forces acting on a particle that is adhering to a bubble can lead to particle detachment (Schulze, 1984). The detachment probability described by Sherrell (2004), equation (6), depends upon the balance between the detachment and the attachment forces.

$$P_d = 1 - \exp\left(-\frac{\sum F_{det}}{\sum F_{att}}\right), \tag{6}$$

Within equation (6):

$\sum F_{det}$ is the sum of the detachment forces, and

$\sum F_{att}$ is the sum of the attachment forces.

Sherrell (2004) proposed equation (7) to obtain P_d, which considers the effect of turbulence on the detachment probability:

$$P_d = 1 - \exp\left(-C\,\frac{\epsilon^{1/3} d_p^{2/3} \rho_p^{1/2}}{\gamma \sin\theta}\right), \tag{7}$$

where C is an empirical constant,
ϵ is the rate of turbulent energy dissipation,
ρ_p is the particle density,
γ is the surface tension, and

High turbulence in a flotation machine may cause particle detachment, possibly explaining the decrease in mass recovery when increasing impeller tip speed (Zhang et al., 2012).

In summary, the particle-bubble interactions in flotation involve collision, adhesion, and detachment events. These sub-processes are influenced by several factors, including hydrodynamic conditions, particle and bubble sizes, surface chemistry, and the balance between the forces promoting adhesion and those causing detachment. Understanding and quantifying these sub-processes is essential for the improvement of flotation performance.

2.3 Key factors influencing hydrodynamics in flotation

Hydrodynamics plays an important role in the efficiency of flotation, a process that selectively separates valuable from gangue minerals based on the differences in hydrophobicity. The comprehension of the key factors that affect flotation hydrodynamics is essential for optimizing the process. This subsection provides an overview of the critical aspects influencing hydrodynamics in flotation, including impeller speed, gas dispersion parameters, cell design, rotor/stator mechanisms, and geometrical aspects of the machine.

2.3.1 Impeller speed

The impeller is a central component of flotation cells, which generates turbulence and energy transference to the pulp, favouring the collision and adhesion of specific mineral particles to air bubbles (Gorain et al., 2000). Manipulating the rotational speed significantly impacts the size and characteristics of the turbulent, quiescent, and froth zones within a flotation cell. Optimal impeller speed is critical for efficient gas dispersion and bubble-particle interactions, with industrial cells typically operating at impeller tip

speeds ranging from 5 to 7 m/s, and up to 9 m/s in some cases (Deglon et al., 2000; Gorain et al., 1996; Zhang et al., 2012).

Impeller speed inversely affects bubble size until a threshold value, beyond which further increases do not reduce bubble size (Amini et al., 2013; Girgin et al., 2006). The impeller speed and the airflow rate significantly impact the rate of energy dissipation in the turbulent region, also affecting the stability of the quiescent-froth interface, which is crucial to control the process selectivity (Mesa et al., 2020). Flotation efficiency depends on an adequate control of the impeller speed due to its influence on gas dispersion, solid suspension, and froth stability.

2.3.2 Gas dispersion parameters

Gas dispersion into small bubbles is a critical hydrodynamic condition in mechanical flotation cells. Three key factors explainining gas dispersion are: bubble size, gas hold-up (ε_g), and the superficial gas velocity (J_g) (Arbiter et al., 1976; Deglon et al., 2000; Vinnett et al., 2014). Bubble size in industrial mechanical cells typically presents high variability, ranging from 1.0 to 4.0 mm (Vinnett, 2023). Bubble size is commonly quatified by the Sauter mean diameter (D_{32}), as defined by equation (8) (Wills & Finch, 2016):

$$D_{32} = \frac{\sum_{i=1}^{n} d_i^3}{\sum_{i=1}^{n} d_i^2}, \tag{8}$$

where n_i is the total number of bubbles in the sample, and
d_i is the diameter of the ith bubble.

Gas hold-up (ε_g), expressed as a fraction or %, is a critical parameter for assessing gas dispersion in a flotation machine. This variable represents the gas fraction by volume, typically estimated independently in the collection and froth zone. The gas hold-up provides insignt into the gas distribution, which directly impacts the flotation performance.

The superficial gas velocity represents the average velocity of the gas phase (air) as it passes through the flotation machine, and can be obtained from equation (9) (Wills & Finch, 2016):

$$J_g = \frac{Q_g}{A_{cell}}, \tag{9}$$

where J_g is the superficial gas velocity,

Q_g is the volumetric gas flowrate, and

A_{cell} is the cross-sectional area of the cell.

The three previously discussed parameters do not fully describe gas dispersion. They collectively define the bubble surface area flux (S_b) in the machine, which represents the rate of bubble surface area entering the cell per unit time and cross-sectional area. This parameter is obtained from equation (10) (Gorain et al., 1997, 1999):

$$S_b = \frac{6\,J_g}{D_{32}}, \tag{10}$$

The characterization of gas dispersion from the bubble surface area flux has proven to be highly effective, with S_b values typically range from 30 to 60 s^{-1} in industrial cells. This parameter has been valuable for scaling-up, optimization, design, and cell selection in metallurgical applications (Gorain et al., 1999).

2.3.3 Cell design

Flotation machines are essential components in mineral processing, playing a crucial role in separating valuable from non-valuable minerals. Machines used in most of the flotation applications are typically classified as either pneumatic or mechanical cells. Pneumatic machines utilize fluid flow to mix solids, liquid, and air. Examples of these machines include flotation columns and Jameson cells. On the other hand, mechanical cells employ a rotary mechanism for mixing and, occasionally, for self-aeration (Kawatra & Young, 2019). Mechanical flotation cells dominate industrial applications due to their versatility and ability to handle a wide range of feed ores. The design of flotation cells is influenced by various factors, including cell geometry, volume, and the impeller-stator system, all of which have a significant impact on the flotation hydrodynamics (Wang & Liu, 2021).

Rotor/stator mechanism

The impeller (rotor) is the main component of a mechanical flotation cell, supplying the energy required for suspending solids, dispersing gas into bubbles, and creating turbulence to improve bubble-particle collision (Gorain et al., 2000). Impeller designs vary based on the cell type, with most featuring a flat circular disc with blades/fingers attached concentrically to the lower section. The stator (stationary component) aims minimizing swirls and vortexes, establishing a quiescent region within the cell conducive to an efficient separation (Schubert, 1999). Investigations into the impeller-stator mechanism often involve computational fluid dynamics (CFD) simulations, and experimental studies to optimize impeller designs, and enhance machine hydrodynamics and flotation kinetics (Wang & Liu, 2021).

Geometrical aspects of a flotation cell

Geometrical aspects of the cell design, such as shape, volume, and aspect ratio, significantly affect the flow profiles and energy disispation within the machine (Gorain et al., 2000). The aspect ratio determines the distribution of the turbulent zones, which impact both the flotation rates and froth recoveries (Tabosa et al., 2016). One of the significant challenges in machine designs is the scale-up of flotation equipment, while optimizing the hydrodynamic conditions. Current methods strongly rely on geometric similarities and dimensional analysis, which may not adequately capture the complexities of the fluid dynamics in large-scale systems (Mesa & Brito-Parada, 2019).

2.4 Flotation reagents

The classification of flotation reagents into collectors, frothers, or modifiers (Kawatra & Young, 2019) is integral to the flotation process. These distinct categories play critical functions for an effective mineral separation. Modifiers are a diverse group of compounds that encompass various reagents beyond collectors or frothers, such as depressants, dispersants, pH regulators, activators, gangue-control reagents, and slime-binding reagents (Kawatra & Young, 2019). Regardless of how flotation reagents are classified,

the main objective remains the same: to select the optimal combination of them that economically and selectively separate the targeted minerals with high recovery.

2.4.1 pH Modifiers/Regulators

Pulp pH significantly influences the flotation performance by modifying the surface properties of minerals and reagents, directly impacting the process selectivity (Fuerstenau et al., 2007). In chalcopyrite flotation, pH is determined by the desired level of pyrite rejection. For ores with high pyrite content, higher pH levels of up to 12 may be necessary to effectively suppress pyrite flotation. Lower pH values of around 8 is typically sufficient for ores with moderate to low pyrite content to achieve the targeted selectivity. The selection of reagent types and concentrations must be carefully considered in conjunction with the optimal pH range to optimize the overall flotation efficiency and selectivity (Wills & Finch, 2016).

Common pH modifiers include lime ($Ca(OH)_2$), soda ash (Na_2CO_3) for increasing the pulp pH, and sulfuric acid (H_2SO_4) or sulfurous acid (H_2SO_3) for decreasing the operating pH. These pH modifiers are essential in sulphide flotation systems (Wills & Finch, 2016).

2.4.2 Collectors

Collectors are organic compounds that render mineral surfaces hydrophobic, promoting their adhesion to air bubbles. They typically consist of a nonpolar hydrocarbon chain (R) and a polar functional group. The polar group favors the adsorption onto the mineral surface, while the hydrocarbon chain orients toward the aqueous phase, imparting hydrophobicity to the mineral, as shown in Figure 7 (Wills & Finch, 2016). The length of the hydrocarbon chain positively correlates with the water repellency and hydrophobicity (Bulatovic, 2007).

Collectors interact with mineral surfaces by chemisorption, forming chemical bonds with surface metal atoms, or by physisorption through electrostatic interactions with the charge of the mineral surface. A monomolecular layer of collector is sufficient to create local adsorption sites. The adsorption is also influenced by the surface roughness, irregular

shapes, and mineralogical composition, which encompasses the variety of minerals present on the surface (Wills & Finch, 2016).

Collectors are classified as cationic or anionic based on their charge. Cationic collectors are preferred at alkaline pH and anionic collectors are suitable for acidic pH conditions (Wills & Finch, 2016). Identifying the most effective collector for a given flotation system is crucial; however, surface contamination affecting collector adhesion is often unavoidable despite efforts to optimize mineral liberation (Nagaraj, 2005).

2.4.3 Frothers

Frothers are essential for stabilizing air bubbles and minimizing their coalescence, thus promoting particle-bubble adhesion. These reagents also alter the surface properties of bubbles to stabilize the froth (Kawatra & Young, 2019; Wills & Finch, 2016). Common frothers contain hydroxyl groups (OH^-) and are constituted of a polar "head" that orients toward the liquid phase and a hydrocarbon "tail" that orients toward the gas phase, as shown in Figure 8 (Wills & Finch, 2016). Frothers stabilize the air-water interface, control the bubble size distribution, generate a stable froth phase, and increase froth mobility (Finch et al., 2008; Wills & Finch, 2016). Each of these functions contribute to the recovery of hydrophobic particles.

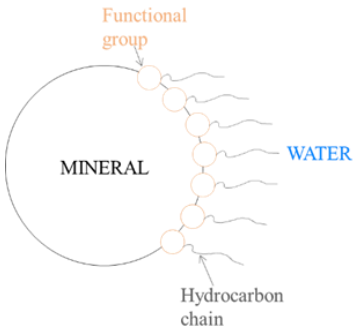

Figure 7. Adsorption of a collector molecule onto a mineral surface, with the hydrocarbon chain extending into the water. Modified from Wills & Finch (2016).

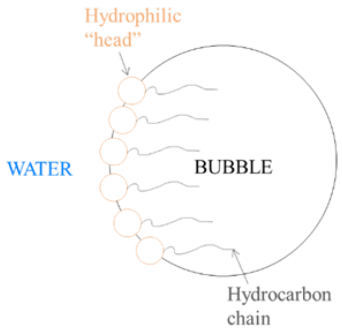

Figure 8. Structure and interfacial orientation of a frother molecule at the air-water interface. Modified from Wills & Finch (2016).

2.5 Flotation kinetics

The first kinetic model in flotation was proposed by Garcia-Zuniga in 1935, who observed that recovery approaches an exponential function over time (Garcia-Zuniga, 1935). Subsequently, Schuhmann (1942) and Mavros & Matis (1992) established criteria for conducting steady-state flotation experiments at laboratory scale. The recovery rate of valuable minerals is a key indicator of flotation efficiency; however, standard procedures to determine flotation rates are not well-established.

Modeling froth flotation is a complex task, as the process consists of multiple subprocesses. In its simplest form, froth flotation can be modeled as equivalent to a chemical reaction between a particle and a bubble, as illustrated in Figure 9 (Wills & Finch, 2016). From this assumption, kinetic modelling of a batch flotation process can be formulated by equation (11) (Mesa & Brito-Parada, 2019).

$$-\frac{dC_p}{dt} = k\, C_b^n\, C_p^m, \tag{11}$$

where k is the rate constant,

C_p is the concentration of particles,

C_b is the concentration of bubbles,

t is the flotation time, and

n and m are respective orders for the bubbles and particles.

In Figure 9, the reactants are the bubble and the particle, and the product is the particle-bubble aggregate. The flotation rate is determined by several factors, including: the concentration of particles and bubbles, the frequency of their collisions, the efficiency of the particle adhesion upon collision, and the stability of the adhesion.

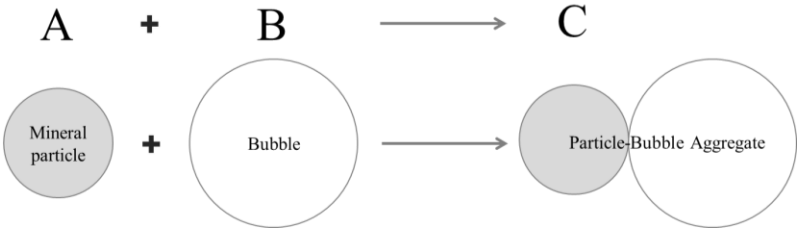

Figure 9. Representation of particle-bubble interactions as a chemical reaction.

The Garcia-Zuniga model of equation (12) (Garcia-Zuniga, 1935) is commonly used in practice, which assumes $n = 1$ in equation (11) and a constant and high concentration of bubbles.

$$R = R_\infty \left(1 - e^{-k\,t}\right), \tag{12}$$

Within equation (12):

R_∞ is the maximum achievable recovery.

To fit a kinetic model, a series of experiments on the investigated ore are performed to obtain the recovery at different time intervals.

2.6 Rate constant as a function of a process variable

Gorain et al. (1995a, 1995b, 1996, 1997, 1998) investigated the effects of impeller type, speed, and air flowrate on flotation performance, while keeping other variables constant. These studies investigated how gas dispersion parameters related to the flotation rate constant. The bubble surface area flux presented a strong correlation with the rate constant, as depicted in Figure 10. Across various impeller types, a consistent linear relationship between k and S_b was found. These findings showed that S_b is a reliable descriptor of the hydrodynamic conditions in a flotation cell, particularly regarding gas dispersion, which plays a crucial role in particle-bubble interactions and flotation kinetics.

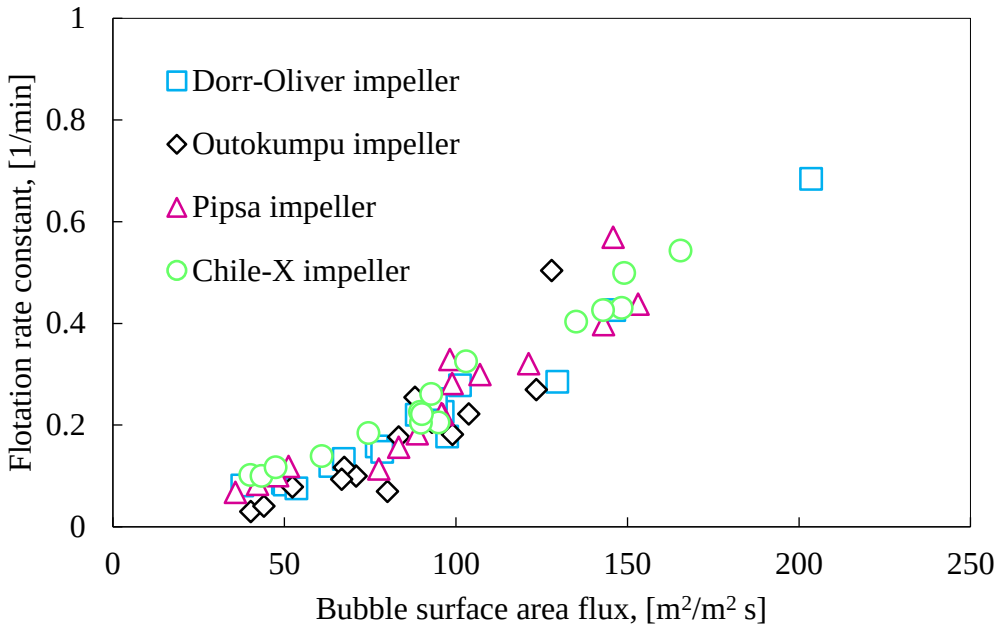

Figure 10. Rate constant versus bubble surface area flux for four different impellers at 16 operating conditions. Modified from Gorain et al. (1997).

The relationship between k-S_b has mathematically been expressed by equation (13) (Gorain et al., 1998):

$$k = P\ S_b, \tag{13}$$

where P is a proportional factor that depends on the mineral floatability, and S_b is the bubble surface area flux.

This expression was extended by Gorain et al. (1999), including a froth recovery factor R_f (overall rate constant divided by the collection rate constant) (Finch & Dobby, 1991).

$$k = P\ S_b\ R_f, \tag{14}$$

The effect of S_b on the rate constant was mainly observed at intermediate and deep froth depths, while shallow froths are better described by equation (13).

2.7 Particle-based modeling in flotation

The evaluation and optimization of flotation processes have typically relied on bulk analysis, which has provided an overall assessment of efficiency and performance. However, this approach has been limited in capturing the complexity of the particle properties, particularly the role of liberation and associations. With the development of advanced analytical and computational techniques, particle-based separation modeling (PSM) has emerged, providing a detailed understanding of the process at the individual particle level (Pereira et al., 2021).

2.7.1 Particle characterization

Particle-based modeling in flotation begins with the comprehensive characterization of individual particles using a scanning electron microscope and energy-dispersive X-ray spectroscopy (SEM-EDS) system; for example, MLA (Pereira et al., 2021). These measurements allow for a detailed characterization of individual particles, including information on:

- **Particle size:** represented by its equivalent circle diameter (ECD), which is the diameter of a circle with the same area as the 2D representation of the particle.
- **Particle shape:** quantified by solidity (2D particle area divided by the respective convex area) and aspect ratio (ratio between the minimum and maximum Feret axes of the 2D particle).
- **Surface composition:** the contribution of different minerals present on the 2D particle perimeter.
- **Model composition:** the content (per area or mass) of different minerals in the 2D particle.

Pre-treatment of the data, such as normalization and de-agglomeration, is essential to ensure accurate and reliable results for subsequent modeling. The specific pre-treatment methods depend on the data type and are discussed in detail by Pereira et al. (2021).

2.7.2 Modeling Approach

PSM aims to create mathematical models to quantify the probability of recovering individual particles in a sample. This objective is achieved as follows (Pereira et al., 2021):

- **Data collection:** representative samples are obtained from each flotation product and analyzed using automated mineralogy.
- **PSM model:** a lasso-regularized multinomial logistic regression, known as PSM, is trained using the data collected. This classification model quantifies the probability of recovering each particle based on its properties, identifying the most suitable coefficients for the different particle features from the frequency at which these particles are found in the different products.
- **Probability of recovering particles:** the trained PSM is used to compute the probabilities of each particle in the feed being recovered in the incremental concentrates or rejected to the tailings. The cumulative sum of these probabilities over a flotation time represents the cumulative recovery of particles with a specific property.
- **Kinetic flotation model fitting:** a classical first-order kinetic model as equation (12) is fitted to each individual particle using non-linear regression, calculating the rate constant and maximum recovery.

In this study, particle-based separation modeling was employed to analyze the flotation performance of specific laboratory-scale separation systems. Methodologies for particle characterization, data collection, and model development and analysis, are described in next chapter.

3 RESEARCH PROCESS

This Chapter provides a comprehensive overview of the methodology employed in this thesis to investigate the impact of hydrodynamic conditions, specifically V_t and J_g, on the flotation performance of a porphyry Cu ore. The methodology encompasses sample preparation, grinding, experimental design, batch flotation tests, and various analytical techniques.

3.1 Material

An ore sample from a porphyry Cu operation in USA was studied. The sample contained on average 1% Cu and 25% Si. The main Cu mineral was chalcopyrite, which was associated with siliceous minerals and pyrite. Figure 11 presents the mineral composition of the feed sample, as determined by MLA, in terms of weight percentage. The primary mineral constituent was quartz, comprising 53.7% of the sample by weight. Orthoclase and other micas accounted for 15.3% and 11.4%, respectively. Muscovite, pyrite, and chalcopyrite were present in moderate amounts of 6.2%, 4.8%, and 3.9%, respectively. Minor mineral phases categorized as "Others", constituted 2.3% of the sample. Kaolinite (1.1%), other silicates (0.7%), other feldspar (0.5%), and other sulfides (0.1%) were present in trace amounts.

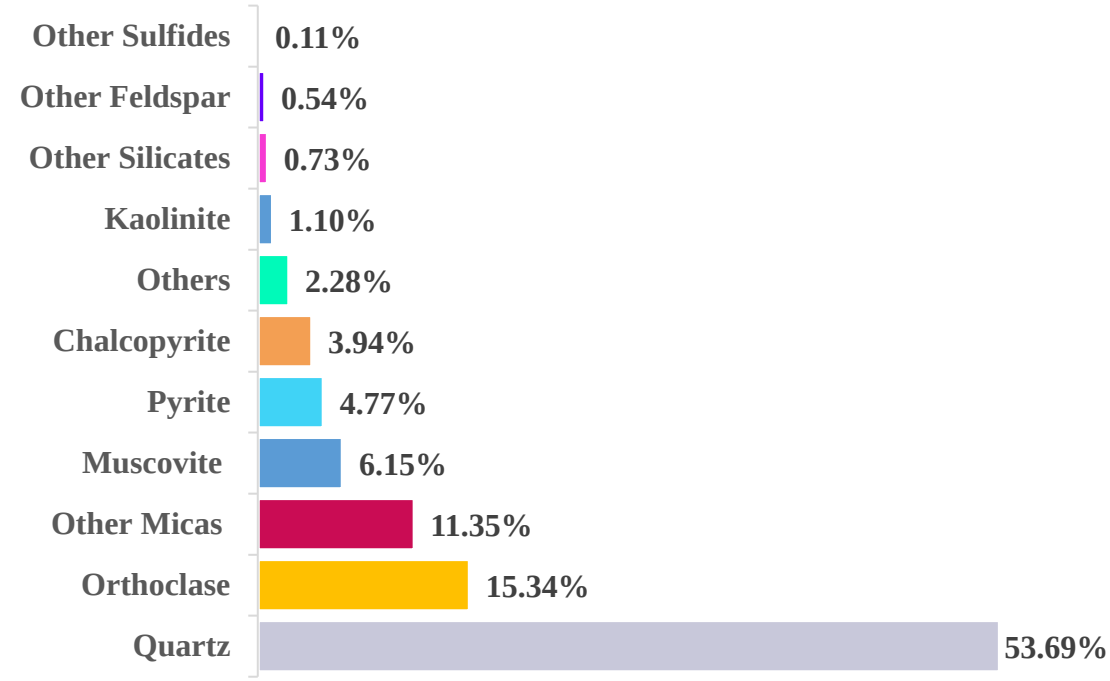

Figure 11. Mineral composition of feed sample by weight from MLA analysis.

3.2 Experiments

This section describes the batch flotation tests conducted at different scales (6 and 35 liters) and their respective procedures. The 6-liter tests were conducted as part of this research, whereas the 35-liter tests were performed in a separate study. Data from the 35-liter tests were provided to investigate the effect of scale on flotation performance.

3.2.1 Batch tests in a 6-liter flotation cell

3.2.1.1 Sample preparation and grinding

The experiments were conducted at the Helmholtz Institute Freiberg for Resource Technology (HIF), where the ore samples were analyzed. The ore samples were subjected to a sequence of splitting steps to obtain representative 1-kg samples suitable for milling. This process ensured the homogeneity and representativeness of the material.

Grinding was performed using a laboratory-scale rod mill equipped with 15 stainless steel rods. The laboratory rod mill has a limited maximum capacity of 1 kg. Therefore, two millings of 1 kg sample were performed before each test. Each test was conducted under

controlled conditions, including a grinding time of 8 minutes and a rotational speed of 960 rpm. A milling time of 8 minutes was determined to achieve the desired particle size distribution, with a d80 of approximately 149 μm (80% of the mass passing 149 μm).

3.2.1.2 Design of experiments (DoE)

A full factorial design was used to investigate the effects of V_t and J_g on the flotation response at two different collector dosages: 3 g/t and 5 g/t. The experiments were carried out separately for each collector dosage. The experimental desing is illustrated in Figure 12 andFigure 13. All experiments were conducted in triplicates.

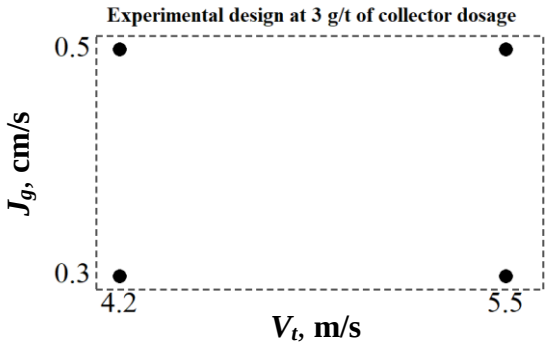

Figure 12. Experimental design at 3 g/t of collector dosage.

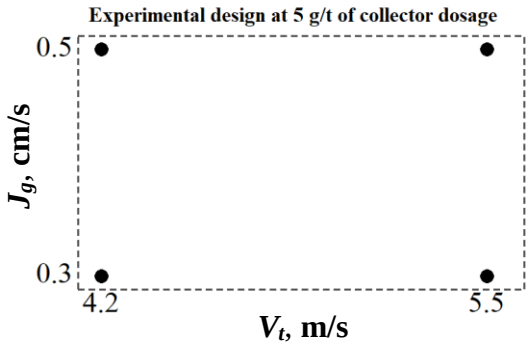

Figure 13. Experimental design at 5 g/t of collector dosage.

By modifying J_g and V_t in the two evaluated datasets, this DoE allowed for investigating the effect of hydrodynamic conditions on the flotation performance, as well as the interplay between the studied hydrodynamic parameters with different collector dosages.

3.2.1.3 Reagents

Isopropyl ethyl thiocarbamate (AERO® 3894 PROMOTER) was used as a collector at 3 g/t and 5 g/t, and OREPREP® X-133 FROTHER was employed as a frother at a dosage of 3 g/t. A 10% lime ($Ca(OH)_2$) slurry was the pH regulator, which was set at 11.3. This reagent scheme was chosen from typical industrial applications.

3.2.1.4 Flotation test

The batch flotation tests were performed in a 6-liter FLSmidth nextSTEP™ flotation cell, varying V_t and J_g. The flotation procedure is schematized in Figure 14. This cell is a cylindrical tank (r = 11 cm, h = 16 cm) equipped with the nextSTEP™ rotor/stator system, as shown in Figure 15A and 15B.

First, pH conditioning was carried out to adjust and stabilize the pH at 11.3 for 180 seconds. The collector was dosage for 120 seconds, and then, a frother was added before each concentrate collection. Four sub-concentrates were taken, C1 was collected for 20 seconds, C2 for 40 seconds, C3 for 60 seconds, and C4 for 120 seconds. Before each concentrate collection, the frother was added in the following sequence: 1.25 g/t for 180 seconds of conditioning before C1; 0.75 g/t for 180 seconds of conditioning before C2; 0.75 g/t for 180 seconds of conditioning before C3; and 0.5 g/t for 60 seconds of conditioning before C4.

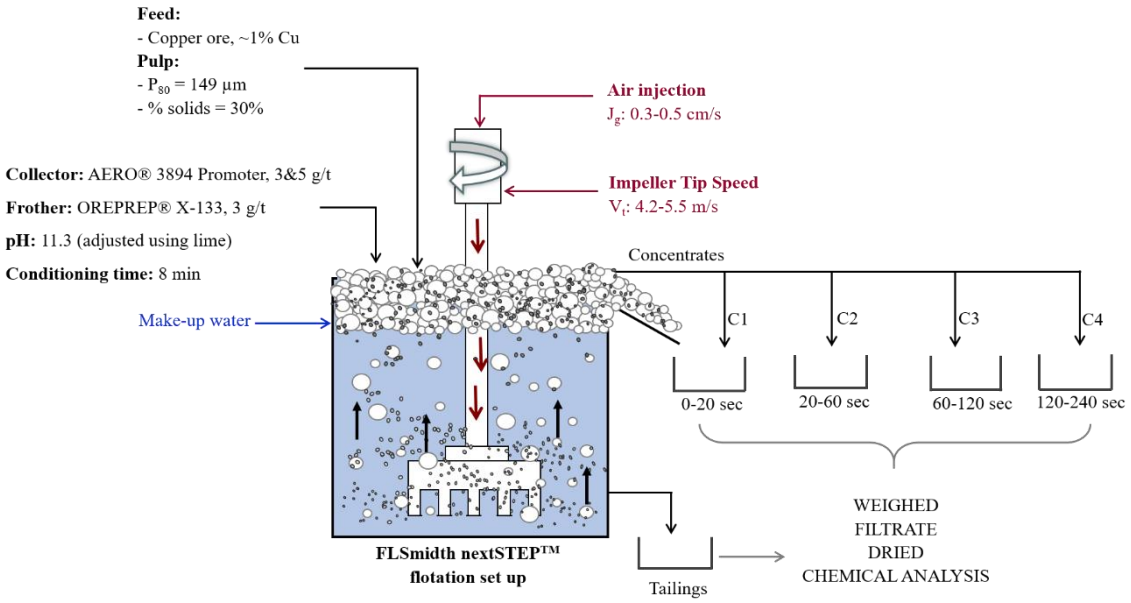

Figure 14. Schematic of the batch flotation procedure.

Auxiliary tools and sensors were integrated in the DigiFlot system of Figure 15C, for continuous monitoring of process parameters. These parameters included pH and temperature. Data from these sensors were automatically collected, time-stamped, and continuously recorded by the DigiFloat system (Lucas et al., 2023).

An air flowmeter (Figure 15E) was employed to set the air flowrate throughout the experiments, whereas a power meter (Figure 15D) was used to measure the power consumption in the flotation tests. The net power consumption attributable to the flotation process was determined by subtracting the power consumption of an empty cell from the recorded values.

After performing the flotation tests, the concentrates and tailings were collected, filtered, dried, weighed, and analyzed.

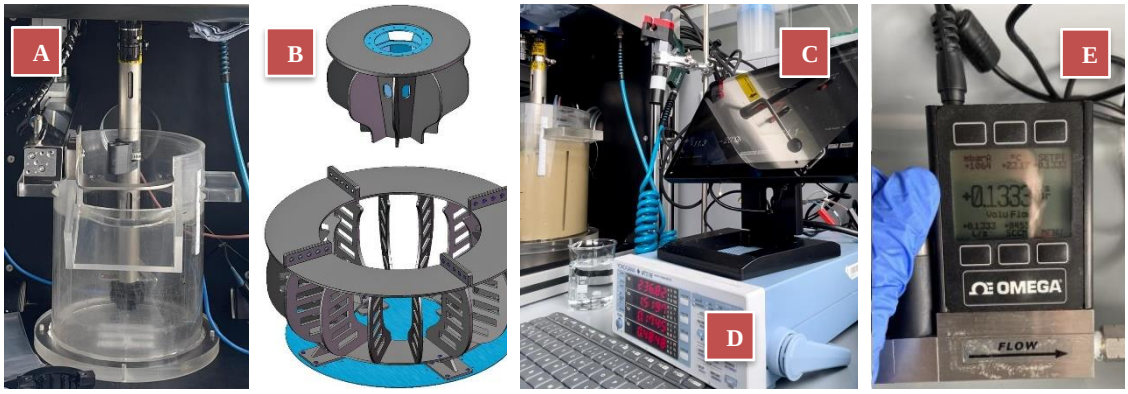

Figure 15. Flotation cell setup and auxiliary equipment used in the experiments. 6-liter cylindrical flotation cell (A); FLSmidth nextSTEP™ rotor/stator system (B); DigiFlot system for process monitoring (C); Power meter (D); and Air flowmeter (E).

3.2.2 Batch tests in a 35-liter flotation cell

The 35-liter tests were performed in a separate study. The data obtained from the 35-liter tests were provided to investigate the effect of scale on the flotation performance.

3.2.2.1 Design of experiments

In this second dataset, V_t and J_g were set at three levels: low, medium, and high values. The DoE for the 35-liter flotation experiments is illustrated in Figure 16.

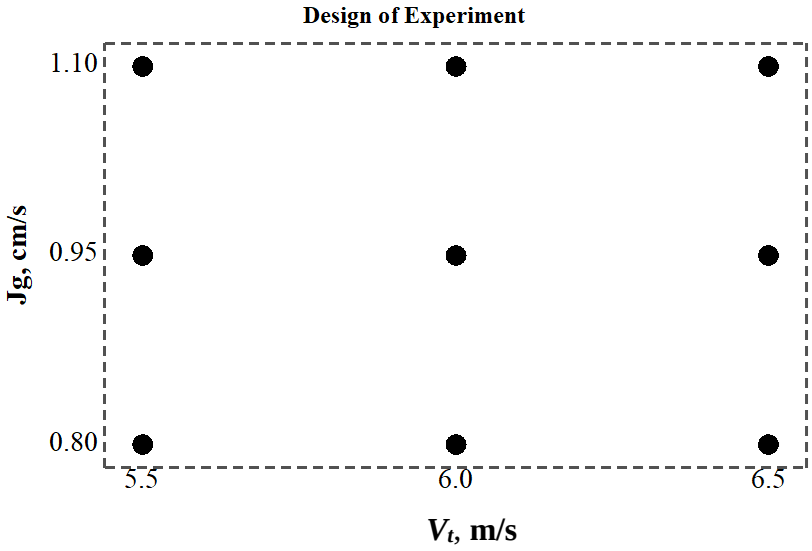

Figure 16. Experimental design of the tests conducted in the 35-liter flotation cell.

3.2.2.2 Flotation tests

The batch flotation tests were conducted in a 35-liter FLSmidth nextSTEP™ flotation cell. Detailed operating conditions are provided in Table 1 compared to those employed in the 6-liter flotation setup.

Table 1. Operating conditions in the batch flotation tests.

Conditions	35-liter flotation cell	6-liter flotation cell	Unit
Sample ore	Porphyry copper ore	Porphyry copper ore	-
Weight of material	12	2	[kg]
Conditioning time	7	8	[min]
pH	11.3	11.3	-
d80	147	149	[µm]
Percent solids	30	30	[% solids]
Collector	AERO 3894® PROMOTER	AERO 3894® PROMOTER	-
Frother	OREPREP® X-133 FROTHER	OREPREP® X-133 FROTHER	-
Collector dosage	5	3 & 5	[g/t]
Frother dosage	4	3	[g/t]
Froth collecting time (cumulative)	0.5, 1.5, 3.5, 6.5, 11.5	0.3, 1.0, 2.0, 4.0	[min]
Base solution $Ca(OH)_2$	-	10	[%]
Products	C1, C2, C3, C4, C5, Tailings	C1, C2, C3, C4, Tailings	-

3.3 Analytic techniques

3.3.1 Portable X-ray fluorescence (pXRF)

pXRF analysis was used to determine the elemental composition of the flotation products of the 6-liter and 35-liter batch flotation tests. The pXRF measurements were conducted using the GeoChem application and DualMining method, which are standardized analytical conditions for determining elemental composition in mineral processing samples. The dried samples were split into representative subsamples. Each sample was triplicated, with manual mixing performed before each measurement to prevent the sedimentation of coarse particles. The averaged data provided insights into the process efficiency in terms of metal recoveries and grades.

3.3.2 Scanning Electron Microscope - Mineral Liberation Analyzer (SEM-MLA)

Samples for MLA characterizations were obtained from the 6-liter batch flotation experiments. Based on the pXRF elemental analysis, samples from the second and third replicates of the DoE were selected for mineralogical analysis. The first replicate was excluded due to the presence of outliers. Two samples from experiments with the same operating conditions were combined and divided using a rotary small-sized splitter and a small riffle splitter, producing 2-g representative subsamples for MLA characterizations. Each sample was mixed with graphite and embedded in an epoxy resin, as shown in Figure 17A.

The samples were coated with a carbon layer using the LEICA EM coater (Figure 17B), with a thickness of approximately 8 nanometers (Figure 17C). In total, 45 samples were prepared for MLA analysis.

Figure 17. Epoxy samples for MLA (A); Carbon coating device (B); An image of carbon-coated epoxy samples (C).

The samples were analyzed by an FEI Quanta 650F scanning electron microscope, equipped with two Bruker Quantax X-Flash 5030 EDX detectors, and processed by Thermo Fischer/FEI's MLA Suite 3.1.4 for automated data acquisition. The GXMAP mode was employed and the probe current was set at 10 nanoamps. The MLA parameters are listed in Table 2.

Table 2. MLA measurement parameters.

Parameters	Value	Unit
Voltage	25	[kV]
Specimen current	10	[nA]
Pixel size	1	[µm/pixel]
Epoxy range	20-250	-
Calibration material	Copper	-
Step size	8	[µm]

3.3.3 Modelling and Evaluation

A modeling approach was applied to the MLA data to simulate and predict individual particle behavior under the studied hydrodynamic conditions in the flotation process. The methodology involved data preprocessing, model training, and validation.

3.3.3.1 MLA data pre-treatment

Back-scattered electron (BSE) and X-ray images of the sample were processed in the MLA-Suite software from Field Electron and Ion Company (FEI). The first step was the mineral classification, based on the spectrum database for known minerals. The mineral

list was able to identify 54 different minerals, and around 100,000 particles per sample, as shown in Figure 18.

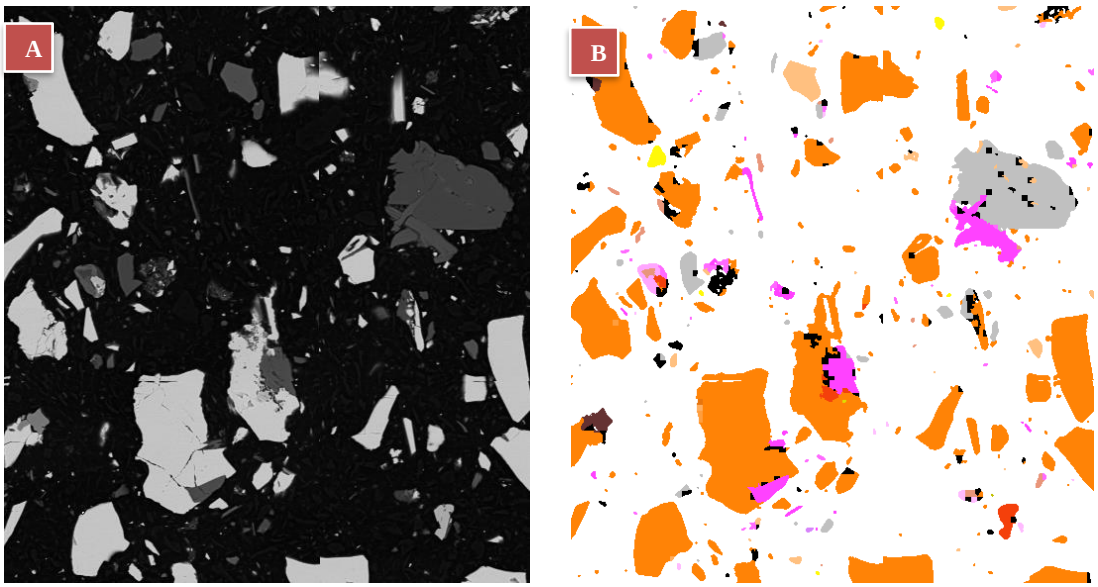

Figure 18. An example of a BSE image of a sample (A); Classified image of the sample (B).

Some agglomerated and overlapped particles are present in the images, as shown in Figure 19 below. The presence of agglomerates (Figure 19A) and clipped particles (particles that are cut off at the edge of the image) may bias the particle characterizations. Therefore, agglomerates and clipped particles were removed, using the preprocessing capabilities. Overlapped particles (Figure 19B) were segmented using built-in algorithms. The RStudio program was then employed to process the large particle datasets.

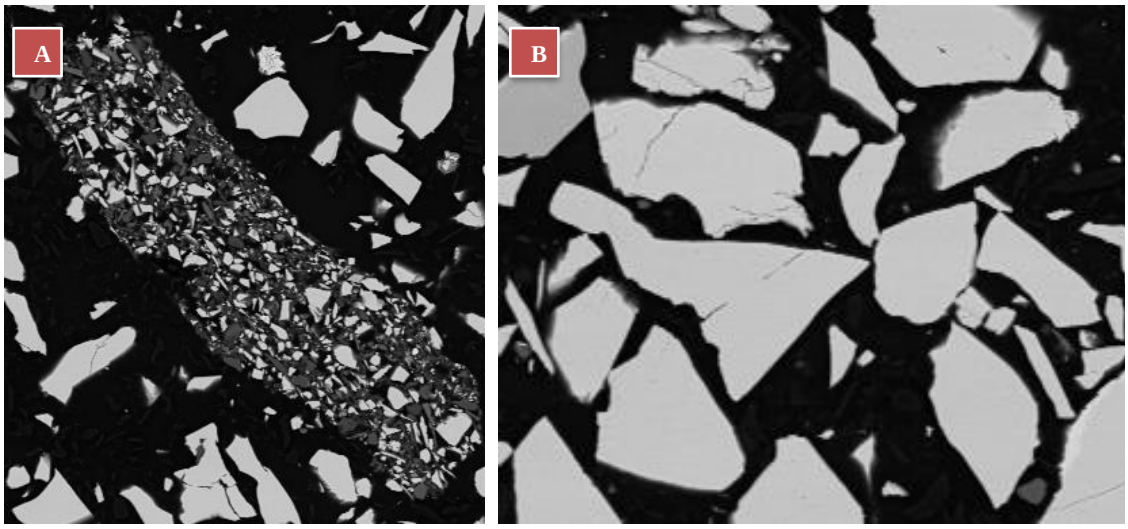

Figure 19. An example of a BSE image of agglomerates (A); An example of a BSE image of overlapped particles (B).

3.3.3.2 Particle-based modeling approach

After the preprocessing the MLA data, the PSM was trained using the particle datasets from the flotation products, each containing approximately 100,000 particles. These particles were characterized by mineralogical composition, shape, size, and density. The training stage employed LASSO-regularized logistic regression, computing response parameters accounting for the influence of the assessed particle properties on the flotation response. The trained model was validated using an independent dataset.

The virtual processing of new feed datasets, using the validated model, predicted the probabilities of each particle to be reported in concentrate time interval or rejected in the tailings. The approach delivered information of the particle distribution probabilities, rate constants, and maximum recoveries for individual particles.

Probability of particles being recovered were calculated by summing the predicted recovery probabilities of each particle in different concentrate products and fitted into a first-order kinetic model, providing insights into flotation kinetics at the single-particle level. The PSM methodology provided a comprehensive understanding of the flotation process at the individual particle level, allowing for evaluating process conditions and improving flotation performance.

4 ASSESSMENT OF THE RESULTS

This section presents the findings from the flotation tests conducted in the 6-liter and 35-liter flotation cells, focusing on the influence of V_t, J_g, and machine scale on the metallurgical performance. Selected samples from the 6-liter tests were analyzed for mineral composition and liberation using MLA. This information aimed the validation of a PSM.

4.1 6-liter flotation tests: regression analysis

Cu recoveries and rate constants were calculated by equations (1) and (13), respectively, based on the pXRF results. The flotation tests were conducted with collector dosages of 3 g/t and 5 g/t. To identify the most significant factors influencing Cu recoveries, concentrate grades, and rate constants, Pareto charts of the standardized effects were generated. These charts are illustrated in Figure 20, 21, and 22 respectively.

The analysis revealed that, at a 95% confidence level ($\alpha = 0.05$), there was insufficient evidence to state that J_g (A), V_t (B), or their interaction term (AB) significantly influenced any of the response variables. This result suggested that the studied factors did not have a critical impact on the flotation performance under the investigated conditions.

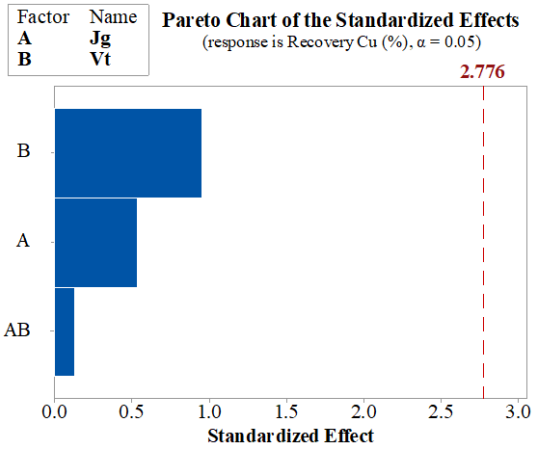

Figure 20. Pareto chart of the standardized effects at α = 0.05, with the response variable being Cu recovery.

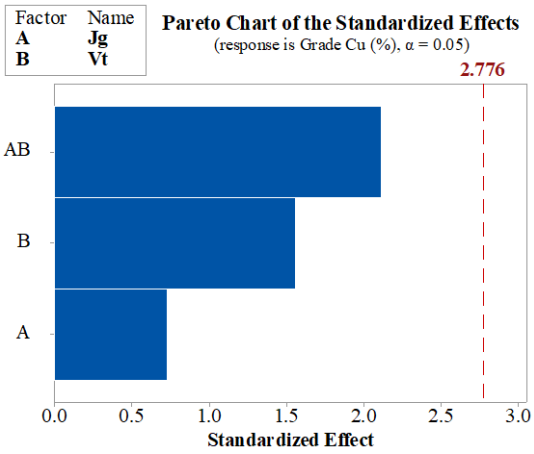

Figure 21. Pareto chart of the standardized effects at α = 0.05, with the response variable being Cu grade.

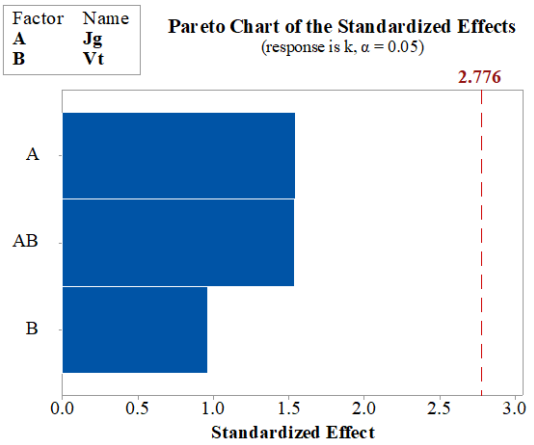

Figure 22. Pareto chart of the standardized effects at α = 0.05, with the response variable being the rate constant.

4.2 35-liter flotation tests: regression analysis

The experiments were also a factorial design, encompassing 9 conditions, along with 2 repeated tests at J_g = 0.95 cm/s and V_t = 6.0 m/s, resulting in 11 experiments. The regression analysis was conducted in two stages: (i) including the interaction between V_t and J_g, and (ii) excluding this interaction to clearly assess the main effects.

4.2.1 Regression analysis with an interaction term

The first regression analysis incorporated the interaction term to evaluate its potential influence on the Cu recovery. The Analysis of Variance (ANOVA) summarized in Table

3. Table 3 shows an F value of 11.1 with a p-value of 0.0047, indicating that the overall regression model is statistically significant. However, the regression coefficients in Table 4 were not statistically significant, as evidenced by their high p-values

Table 3. ANOVA for the regression model.

Source	Degrees of freedom	Sum of square	Mean square	F value	P value
Regression	3	497.9365	165.9788	11.1215	0.0047
Residual	7	104.4685	14.9214		
Total	10	602.4050			

Table 4. Regression coefficients and their statistics.

Term	Coefficient	Standard error	t-stat	P value
Intercept	158.305	148.989	1.063	0.316
J_g	-2.731	2.611	-1.046	0.323
V_t	-0.021	0.087	-0.240	0.816
$J_g V_t$	0.001	0.002	0.789	0.451

4.2.2 Regression analysis without an interaction term

Given the non-significance of the interaction term, a second regression model was analyzed, excluding this interaction. The residuals plot Appendix (1) shows the differences between the observed and predicted Cu recovery values. The residuals appear to be randomly dispersed around zero, indicating that the model's assumptions are likely satisfied. The results, presented in Tables 5 and 6, showed that V_t and J_g were statistically significant. J_g had a coefficient of -0.68, indicating a negative effect on the flotation performance, while V_t had a coefficient of 0.05, indicating a significant although low positive effect.

Table 5. ANOVA for regression model

Source	df	Sum of square	Mean square	F value	P value
Regression	2	488.6515	244.3257	18.1828	0.0013
Residual	8	113.7535	14.2192		
Total	10	602.4050			

Table 6. Regression coefficients and their statistics

Term	Coefficient	Standard error	t-stat	P value
Intercept	42.01	20.941	2.006	0.073
J_g	-0.68	0.173	-3.912	0.003
V_t	0.05	0.011	-4.366	0.001

Figure 23 illustrates the relationship between measured Cu recovery and modeled Cu recovery. The red dashed line represents the y=x line, indicating perfect agreement between measured and modeled values. The blue crosses represent individual data points, showing how the modeled Cu recovery compares to the actual measured Cu recovery. The data points generally follow the y=x line, indicating good model performance, although some deviations are present.

Note that, for Cu grade and rate constant, J_g and V_t were not significant factors in this model.

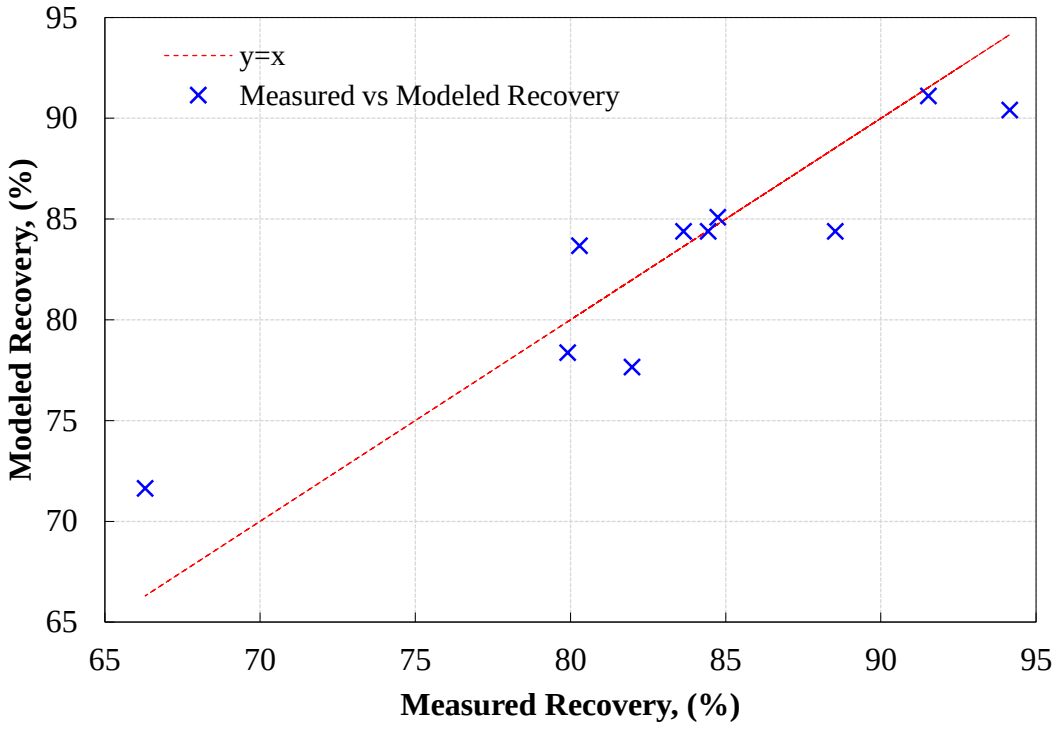

Figure 23. Comparison of measured vs. modeled recovery.

4.3 Analyzing scale variations: hydrodynamics in the 6-liter and 35-liter flotation cells

The regression analysis of the 6-liter and 35-liter flotation tests revealed a notable difference in the statistical significance of the studied factors. In the 6-liter cell, neither J_g nor V_t significantly influenced the response variables at a 95% confidence level. This result suggested that in the small-scale cell, hydrodynamic conditions may not substantially impact flotation performance. Previous studies supported this finding, indicating that the impact of turbulence and hydrodynamics on flotation performance significantly varies with cell size (Amini et al., 2013; Tabosa et al., 2016).

In contrast, the 35-liter cell experiments demonstrated statistically significant effects of V_t and J_g on Cu recovery, with J_g exhibiting a negative influence and V_t showing a positive impact. These findings suggest that in large-scale cells, hydrodynamic conditions play a role on flotation performance, where optimal J_g and V_t are crucial for improving recovery rates (Amini et al., 2016).

Several factors may explain the difference in statistical significance between the two cell sizes. The larger slurry volume in the 35-liter cell provides a more representative sample of the ore body, reducing the sources of experimental error (Napier-Munn, 2020).

Despite the lack of statistical significance in the 6-liter cell, small-scale machines can still provide valuable insights into the flotation process. To further investigate the flotation performance in the 6-liter cell, representative samples of the flotation products were analysed by MLA. When integrating mineralogical results with PSM, a deeper understanding of mechanisms governing the overall flotation performance is achieved at individual particle level.

4.4 Comparative analysis of pXRF and MLA results

Figure 24 presents a comparative analysis of Cu recoveries and rate constants measured by two different analytical techniques: pXRF and MLA. Four subplots (A, B, C, and D), are depicted, showing the Cu kinetic responses under different conditions of J_g and V_t.

Figure 25 presents the Cu grades (%) measured by pXRF and MLA at different operating conditions for concentrates C1, C2, C3, and C4.

In Figure 24A, *k* was 1.04 min^{-1} from pXRF measurement and 0.98 min^{-1} from MLA data. The higher *k* estimations using pXRF across all conditions suggested potential differences in sensitivity or calibration between the two techniques. Nevertheless, the consistent results confirmed the reliability of the analysis techniques, which made it possible for the use of only pXRF in the 35-liter cell tests.

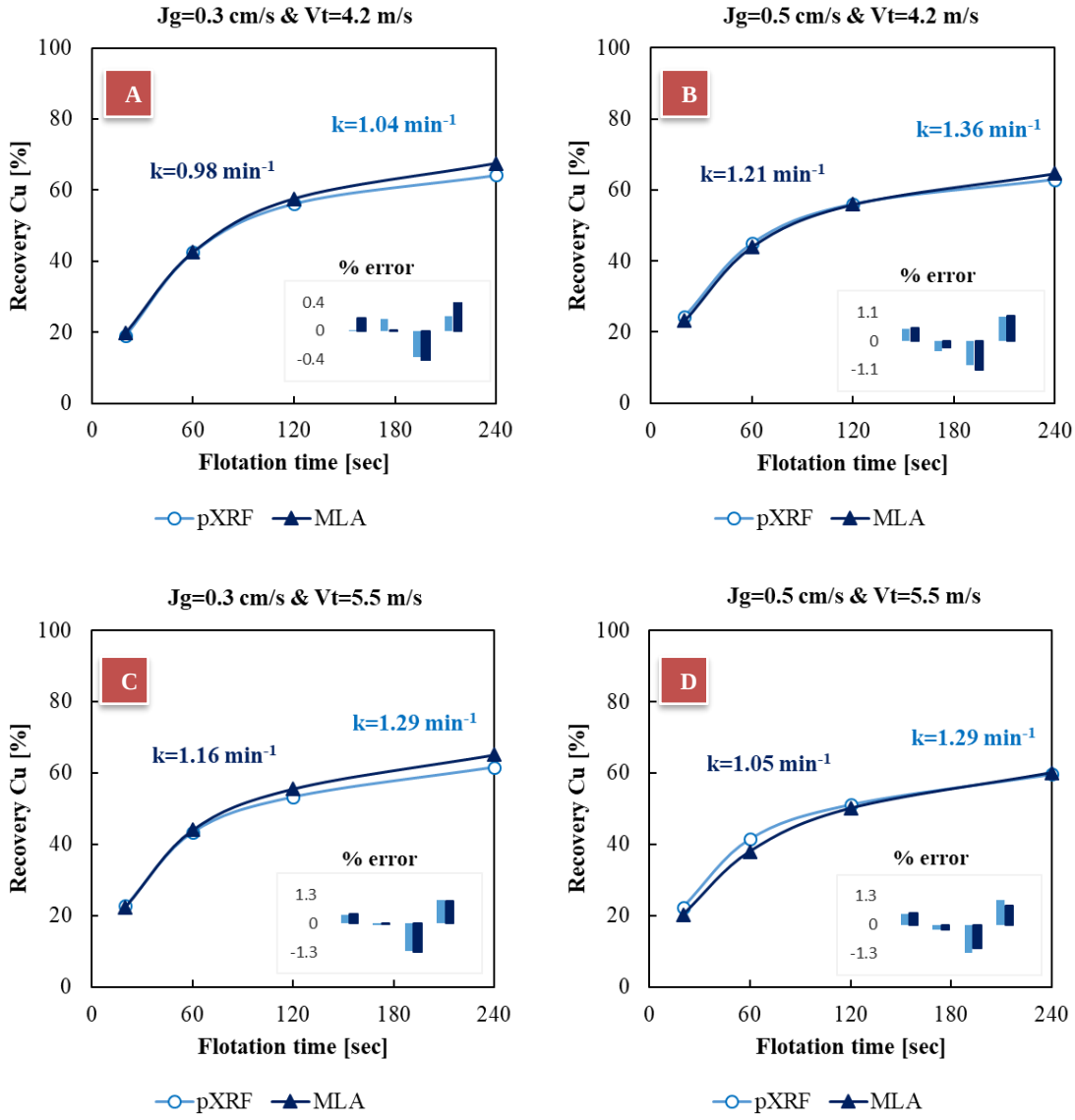

Figure 24. Comparison of Cu recoveries and rate constants obtained from the pXRF and MLA measurements.

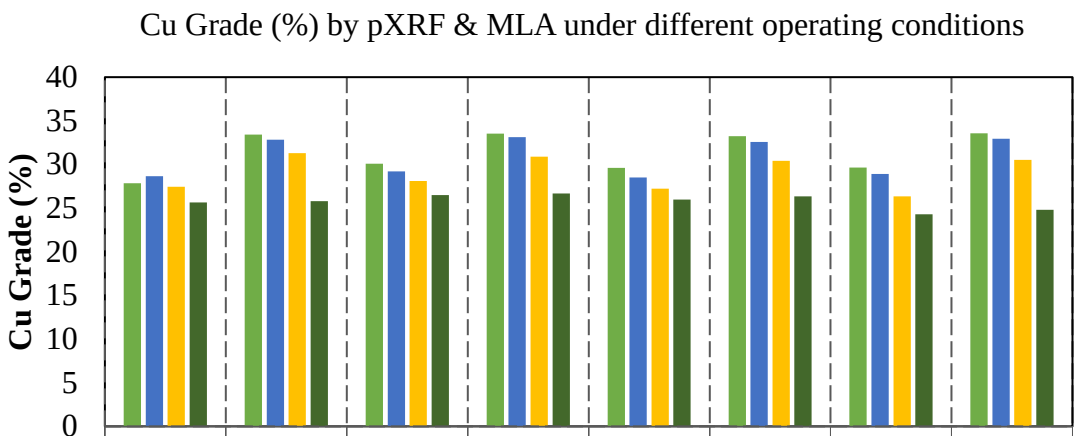

	pXRF	MLA	pXRF	MLA	pXRF	MLA	pXRF	MLA
	Jg=0.3 cm/s Vt=4.2 m/s		Jg=0.5 cm/s Vt=4.2 m/s		Jg=0.3 cm/s Vt=5.5 m/s		Jg=0.5 cm/s Vt=5.5 m/s	
C1	27.83	33.40	30.09	33.54	29.62	33.22	29.63	33.57
C2	28.64	32.84	29.22	33.12	28.49	32.57	28.92	32.93
C3	27.46	31.30	28.10	30.90	27.24	30.41	26.34	30.52
C4	25.66	25.78	26.49	26.67	25.99	26.36	24.30	24.80

Figure 25. Comparison of Cu grades (%) measured by pXRF and MLA at different J_g and V_t, for concentrates C1, C2, C3, and C4.

4.5 Particle-based separation modeling

All plots presented from this point onward were created using particle-based separation modeling, integrated with MLA data. For the 6-liter tests, two DoEs evaluated the impact of V_t and J_g on flotation at collector dosages of 3 g/t and 5 g/t, respectively. To maintain clarity and conciseness, this section analyzes the DoE findings at the 3 g/t of the collector. Results at 5 g/t are provided in Appendix (2) for reference and completeness.

4.5.1 Model mineralogy

The initial data obtained from automated mineralogy is the mineralogical assemblage. The minerals of the ore were grouped as follows: chalcopyrite, Cu-sulfides, pyrite, other sulfides, quartz, oxides, other semi-soluble salt-type minerals (abbreviated as SSSM), silicates, and micas (Table 7).

Table 7. Groups of minerals in the studied ore.

Groups	Minerals
Chalcopyrite	
Cu-sulfides	Bornite, chalcocite, tennantite
Pyrite	
Other sulfides	Molybdenite, galena, pentlandite, pyrrhotite
Quartz	
Oxides	Ilmenite, hematite, rutile, magnetite, corundum
SSSM	Apatite, calcite, dolomite, fluorite, siderite
Silicates	Orthoclase, kaolinite, albite, plagioclase, illite
Micas	Muscovite, biotite

Figure 26 displays the modal mineralogy of four analyzed feed samples. Quartz, silicates, and micas were the more massive minerals in all four samples. Figure 27 shows some variability when analyzing the compositional distribution on a size-by-size basis. These distributions were obtained by back-calculating the flotation feed from the products. The dominant size class across all sets was the -300/+100 μm fraction, followed by the -100/+50 μm class, with lower fractions in the -50/+25 μm and -25 μm classes. The distribution patterns suggested that coarse particles are more prevalent across all sets. The chalcopyrite content in the coarsest fraction was lower in Set 2 (approx. 50 wt. %), with pyrite having the highest content (approx. 70%) in this sample and size fraction. Samples from Sets 1, 3, and 4 did not present critical differences in the size-by-composition results. Results from Figures 26 and 27 supported the sampling and analytical routines, as the observed variability was expected for the studied low-grade ore.

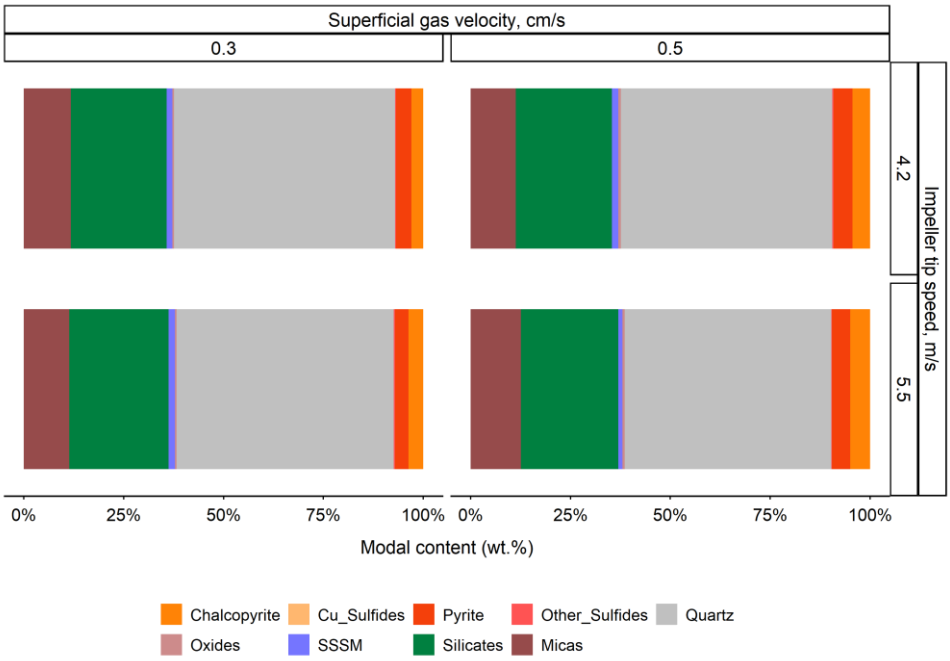

Figure 26. Modal mineralogy of the four investigated feed samples.

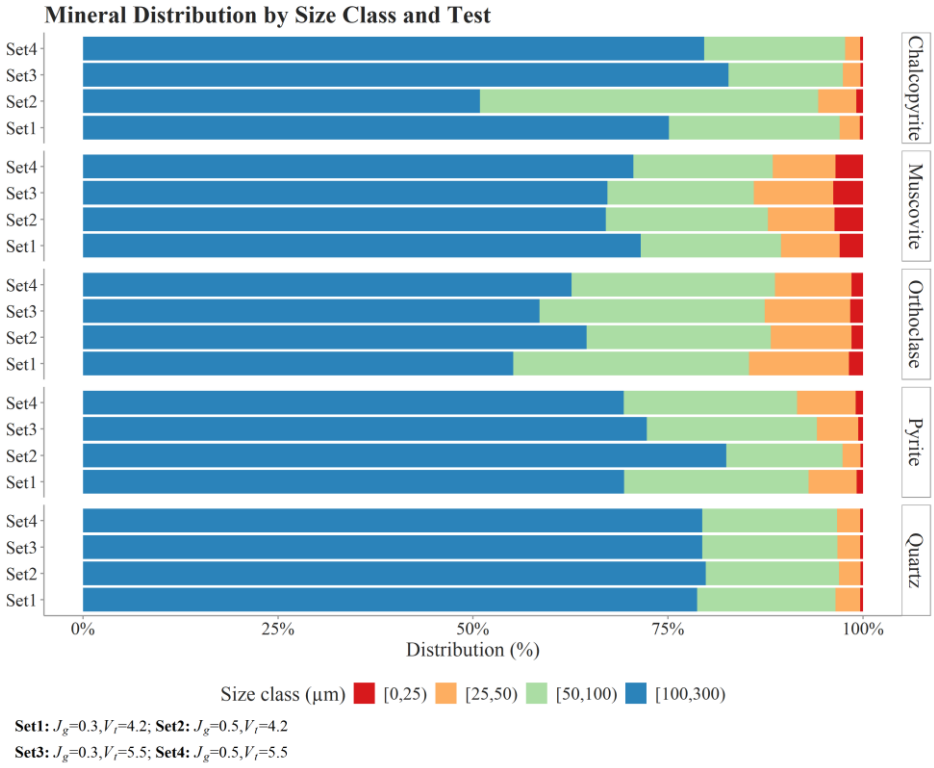

Figure 27. Size-by-composition distribution of the mineral phases in the flotation feed, based on back-calculated data.

Figure 28 presents the MLA results for the chalcopyrite association across the tested samples. As expected, the fraction of locked particles increased with particle size. Liberation refers to the relative surface content of the assessed mineral. On average, up to 70% (by mass) of chalcopyrite was fully liberated (>90% liberated). Approximately 20% of chalcopyrite presented 50%-90% of liberation, and around 10% of chalcopyrite was associated with other minerals, such as quartz, pyrite, and others. Given the high fraction of fully liberated chalcopyrite, the subsequent graphs are focus on chalcopyrite particles with levels of liberation greater than 95%.

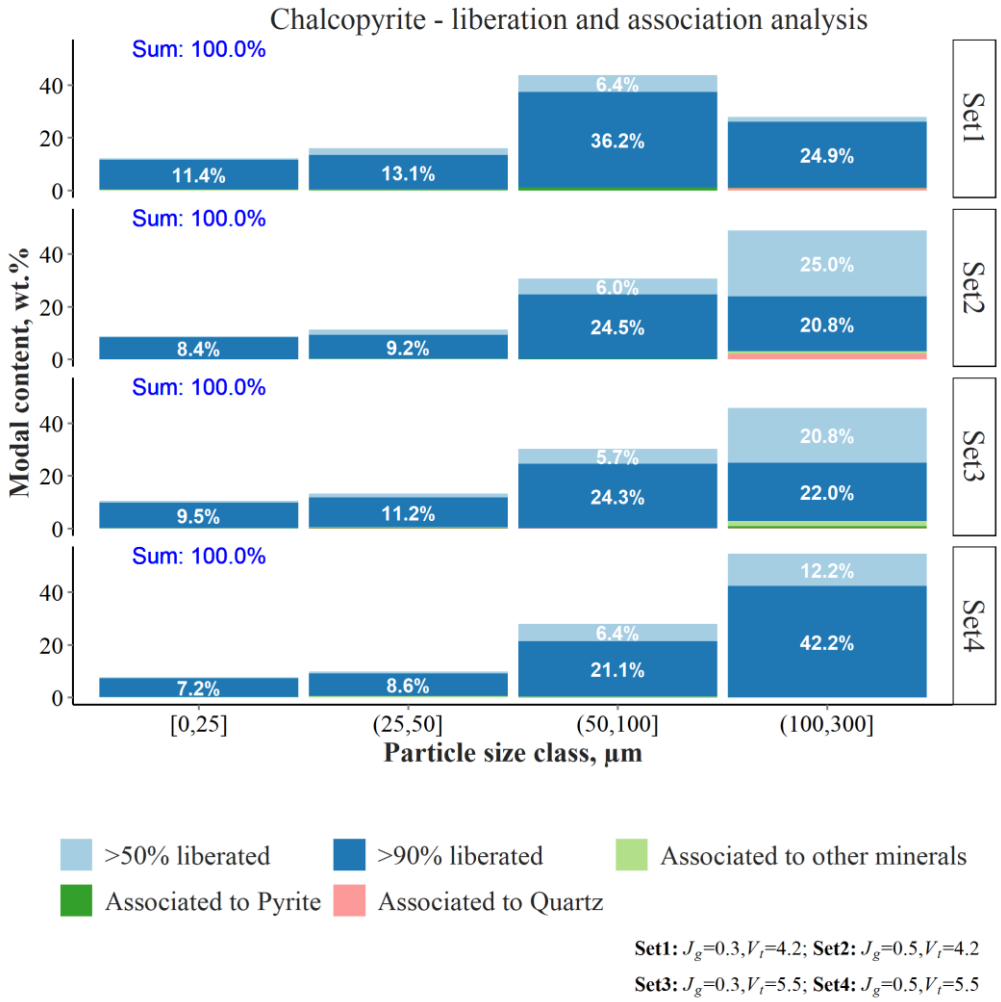

Figure 28. Based on back-calculated feed data, Chalcopyrite liberation and association per size class, showing the mass content.

4.5.2 Effect of V_t on Cu recovery

Figure 29 illustrates the relationship between particle size and chalcopyrite recovery at different V_t and J_g. Increasing V_t from 4.2 to 5.5 m/s, controlling J_g at 0.3 cm/s, resulted in improved chalcopyrite recovery and a narrow concave response as a function of particle size. At a J_g of 0.5 cm/s, increasing V_t also enhances chalcopyrite recovery but produces a wider concave response with respect to particle size.

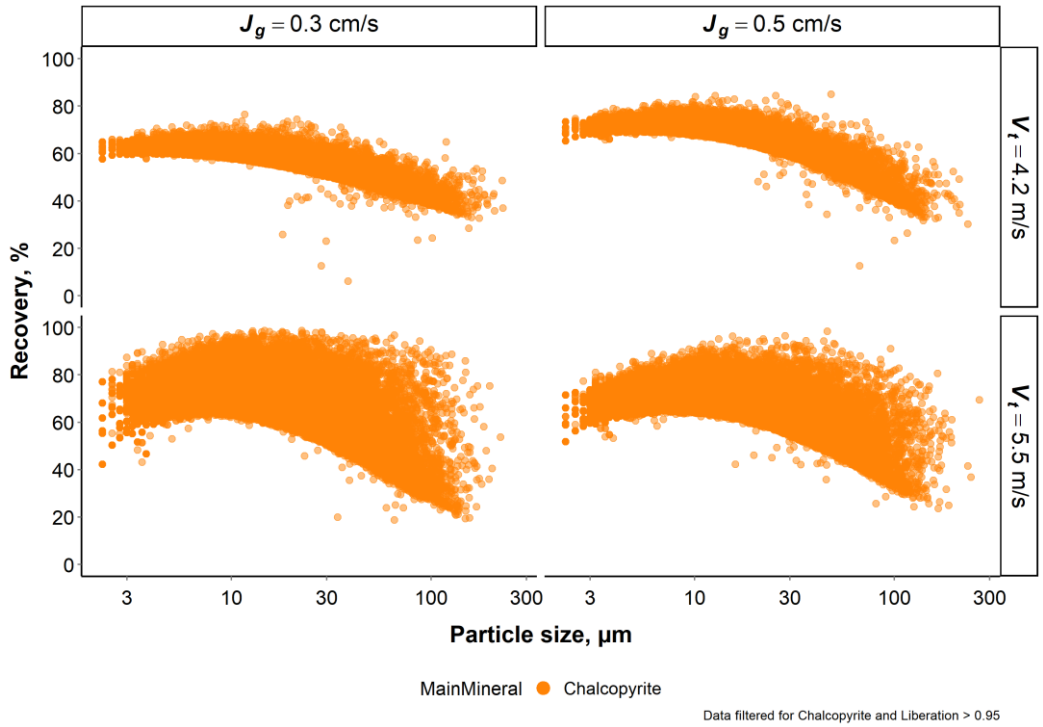

Figure 29. Fully liberated chalcopyrite recovery-particle size relationship under different hydrodynamic conditions. Figure 30 and Figure 31 show the distribution of the probability of recovering particles across different size classes (-25 µm, -50/+25 µm, -100/+50 µm, and -300/+100 µm) using violin plots. These plots present the effect of changing V_t from 4.2 m/s to 5.5 m/s at J_g = 0.3 cm/s and J_g = 0.5 cm/s, respectively. The green and orange colors denote Cu recoveries at V_t = 4.2 m/s and V_t = 5.5 m/s, respectively.

From Figures 30 and 31, as particle size increased, a decrease in recovery was observed, mainly related to particle-bubble detachment caused by the higher turbulence and shear forces (Schubert, 1999). Higher recoveries were observed in the finer classes due to

higher collision and adhesion efficiencies. In overall, all size classes, as V_t increased, an increase in the recovery was observed, and the variation of recovery was higher. The increase in the recovery is mainly related to more frequent particle-bubble collisions at higher V_t (Deglon et al., 2000; Jameson, 2012). In additionally, higher V_t favours the formation of smaller bubbles, which have higher surface-area-to-volume ratios, improving the rate constant, especially for highly liberated particles (Deglon et al., 2000; Jameson, 2012). Higher V_t also keeps particles suspended, preventing settling.

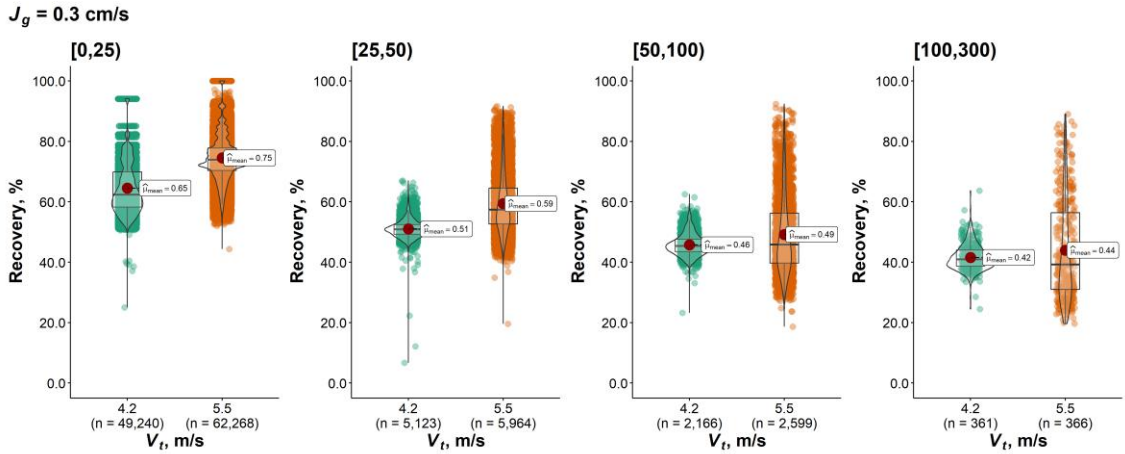

Figure 30. Violin plot of the size-by-size chalcopyrite recovery as a function of V_t, at a constant J_g = 0.3 cm/s.

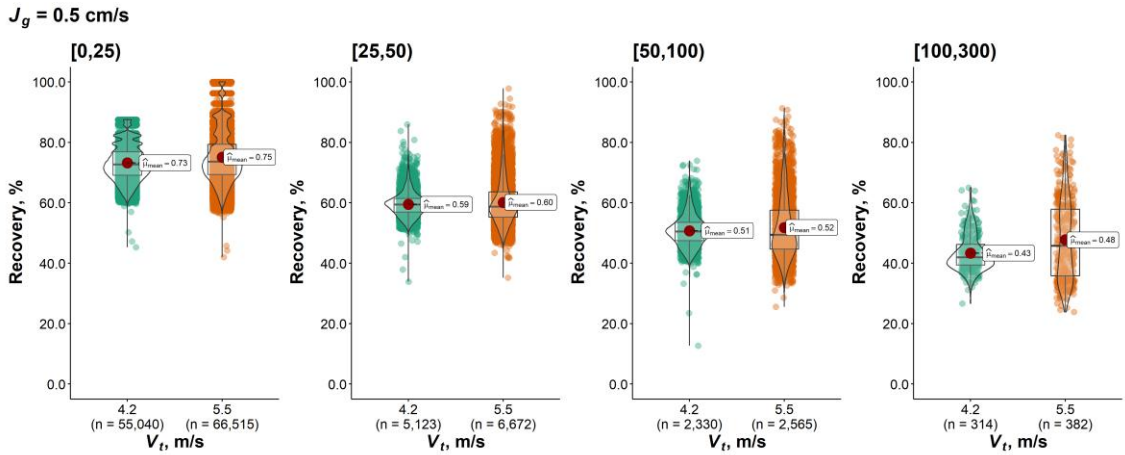

Figure 31. Violin plot of the size-by-size chalcopyrite recovery as a function of V_t at a constant J_g =0.5 cm/s.

4.5.3 Effect of J_g on recovery

The effect of increasing J_g from 0.3 to 0.5 cm/s on chalcopyrite recovery was also studied at constant V_t. Figures 32 and 33 present the probability of particles being recovered on a size-by-size basis for these two J_g values, respectively.

A cursory look at the Figures 32 and 33, the mean recovery ($\hat{\mu}_{mean}$) decreased as particle size increased. In Figure 32, at higher gas rates (J_g = 0.5 cm/s), the recoveries slightly increased. When J_g was increased to 0.5 cm/s, with V_t = 5.5 m/s (Figure 33), the effect of the air rate on recovery was negligible. This suggests that at high V_t, the system's hydrodynamics dominate flotation performance, reducing the influence of J_g. High turbulence and efficient mixing at V_t = 5.5 m/s enhance bubble-particle interactions, leading to a recovery plateau despite increased J_g. Thus, additional air rate increases may not significantly enhance recovery.

The low impact of J_g on recovery at high V_t might be attributed to several factors. High impeller speeds generate significant turbulence and mixing, enhancing bubble dispersion and particle attachment, which diminishes the effect of increased J_g. High V_t produces smaller, more uniform bubbles with a higher surface area-to-volume ratio, enhancing flotation efficiency and reducing the need for higher J_g. Consequently, flotation kinetics and bubble-particle interactions are likely already highly efficient at high V_t, rendering further increases in J_g less effective. These factors underscore the importance of balancing hydrodynamic conditions to achieve maximum flotation efficiency.

The results indicated that the effect of increasing J_g from 0.3 to 0.5 cm/s on chalcopyrite recovery depends on V_t. At lower V_t of 4.2 m/s, increasing J_g more visibly enhanced recovery, due to an increase in S_b, which facilitates better particle collection (Gorain et al., 1997) and froth mobility (Finch & Dobby, 1991). However, at V_t = 5.5 m/s, the impact of increasing J_g on recovery is minimal, due to the detrimental effects of an excessive increase in turbulence and shear forces, which promotes particle-bubble detachment (Schubert, 1999). These findings are consistent with previous results reported in literature that has highlighted the complex interplay between S_b, particle size, and hydrodynamic conditions in flotation (Gorain et al., 1997; Schubert, 1999).

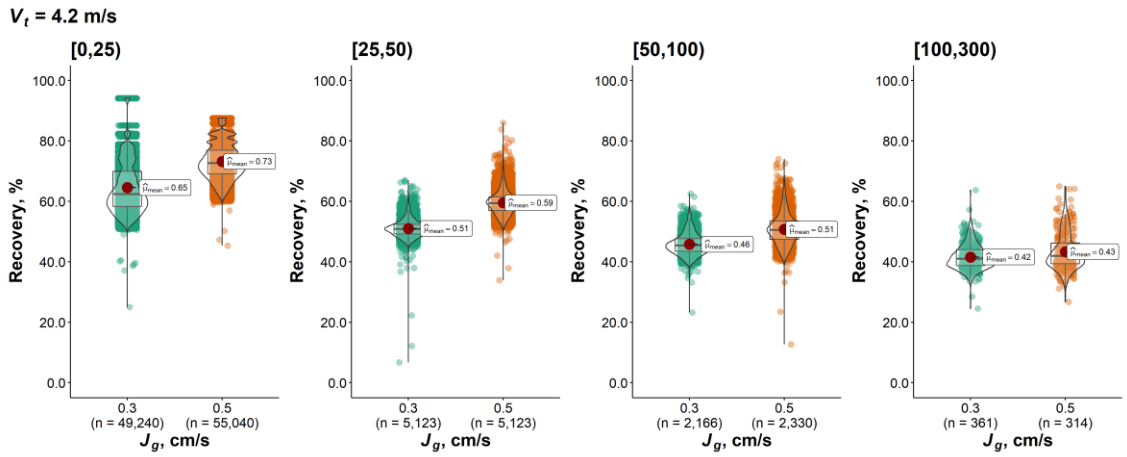

Figure 32. Violin plot of the size-by-size chalcopyrite recovery as a function of J_g at a constant V_t = 4.2 m/s.

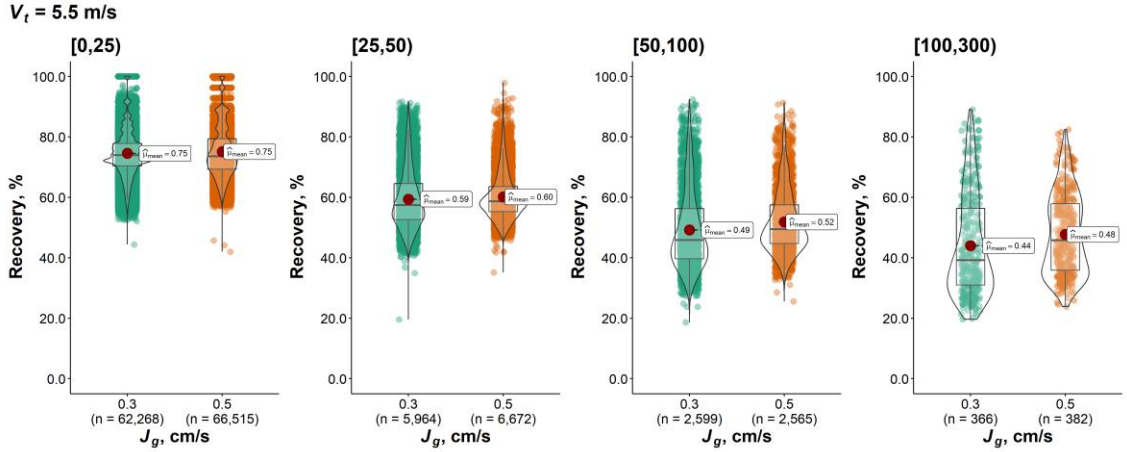

Figure 33. Violin plot of size-by-size chalcopyrite recovery as a function of J_g at a constant V_t = 5.5 m/s.

4.5.4 Effect of J_g and V_t on rate constant (k)

Figure 34 shows the effect of particle size on the rate constant for the liberated chalcopyrite, at the different combinations of V_t (4.2 or 5.5 m/s) and J_g (0.3 or 0.5 cm/s). The k value was low for fine particles, increasing with particle size and reaching a maximum of around 30 μm. A monotonic decrease was observed thereafter. This trend was consistent with previous research findings, from which k typically increases as a function of particle size until an optimum size is reached (Jameson, 2012).

The rate constant was lower at V_t = 4.2 m/s and J_g = 0.5 cm/s compared to V_t = 4.2 m/s and J_g = 0.3 cm/s, which may have been caused by insufficient dissipation energy to disperse the gas and promote particle-bubble interactions. Thus, larger and less stable bubbles may have favoured the particle detachment when reaching the pulp-froth interface (Deglon, 2005; Gorain et al., 1995a).

The influence of V_t and J_g on flotation is shown in Figure 35. With a decrease in J_g, the grade-recovery curve shifts to the upper right corner, however negatively affecting the flotation kinetics. Indeed, the particles float slower, but the grade is highly affected due to less entrainment at a lower J_g. Furthermore, as the J_g increases, so do the kinetics of the particles while still reaching an asymptote. This means that it is useless to keep increasing the J_g in the hope of floating faster and better.

For V_t and J_g, the grade generally increases with a decrease in those variables, which also leads to a decrease in *k*. In contrast, as these variables increase, an increase in recovery can be seen as well. So there exists a trade-off between those parameters to achieve balance in terms of Cu grade and recovery. The relationship between hydrodynamic variables and flotation kinetics depends not only on the pulp phase but also on froth properties, i.e. froth stability, froth structure, and bubble size, which are influenced by the V_t and the J_g.

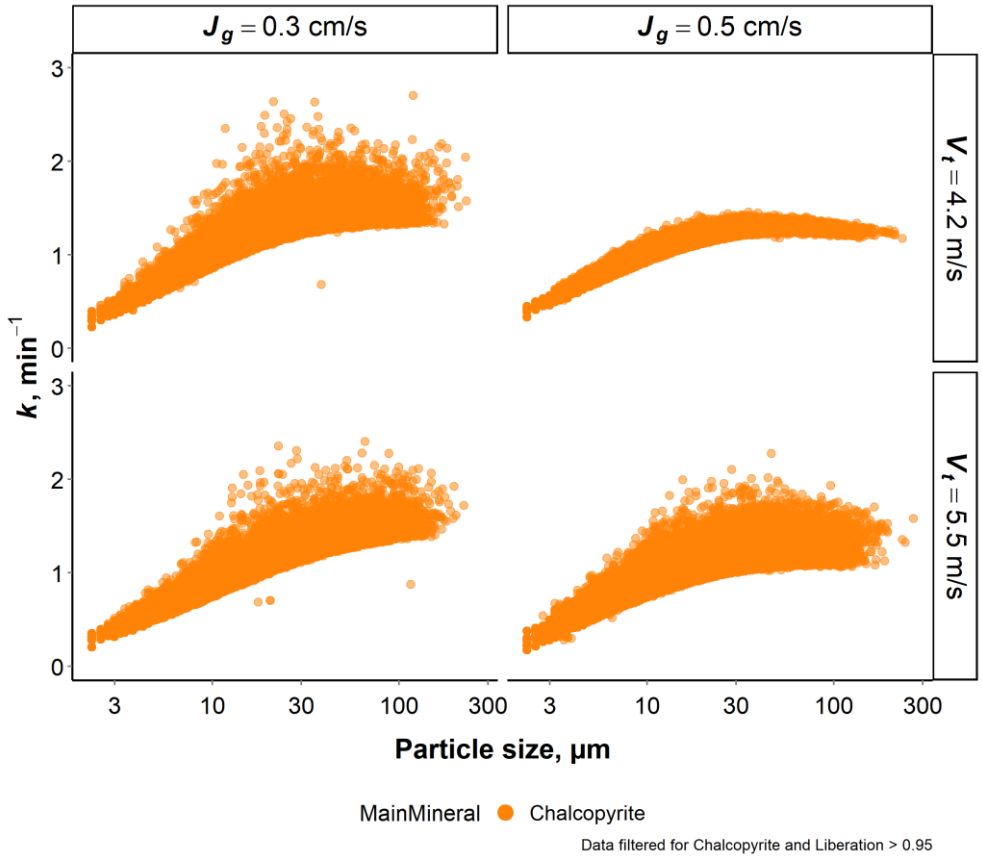

Figure 34. Effect of particle size on the rate constant for liberated chalcopyrite at different combinations of V_t and J_g.

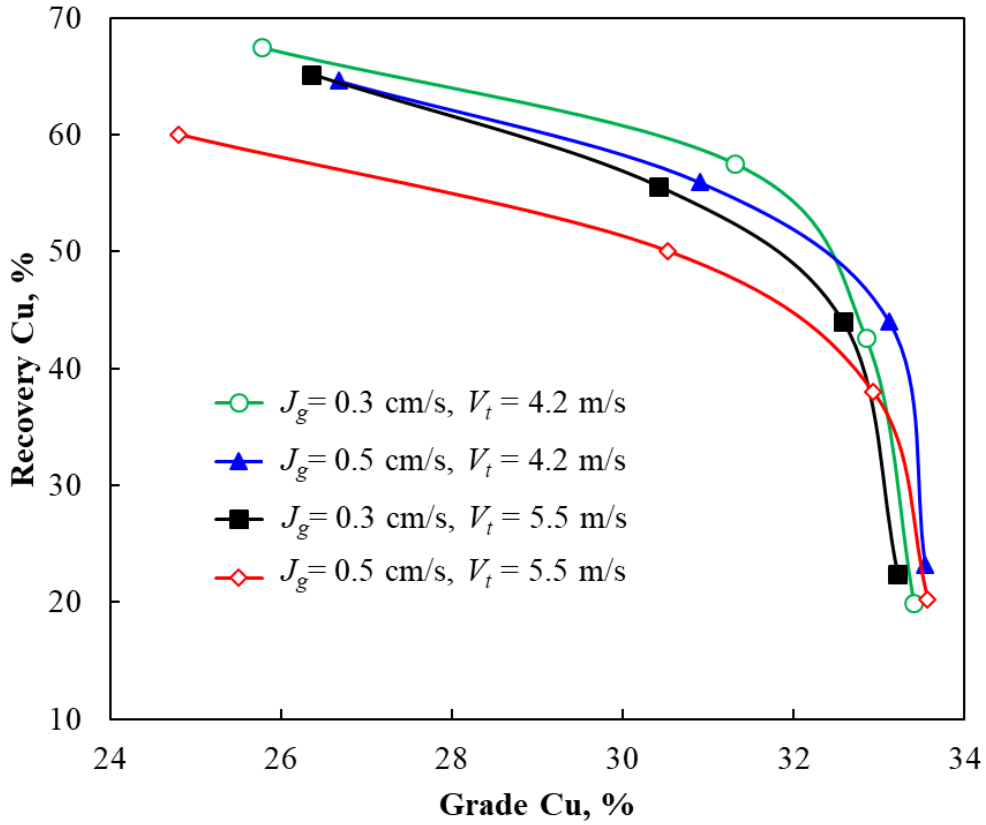

Figure 35. Effect of hydrodynamic variables on recovery and grade of Cu

The investigation of the flotation tests in 6-liter and 35-liter cells provided insights into the influence of hydrodynamic variables V_t and J_g on metallurgical performance. In the 6-liter tests, neither V_t nor J_g significantly impacted Cu recovery, concentrate grade, or rate constants, suggesting a minimal effect of hydrodynamic conditions in smaller cells. Conversely, in the 35-liter tests, V_t and J_g significantly influenced the flotation recovery, with J_g exhibiting a negative effect, and V_t a positive impact. Thus, hydrodynamic conditions play a more critical role in flotation performance in larger cells. Furthermore, the MLA-based particle separation modeling underscored the intricate interplay of mineral liberation, particle size, and flotation kinetics, emphasizing the need to balance hydrodynamic conditions for optimal performance.

5 CONCLUSIONS AND RECOMMENDATIONS

This study investigated the impact of hydrodynamic conditions, specifically impeller tip speed (V_t) and superficial gas velocity (J_g), on the flotation performance of a porphyry copper ore. Two flotation scales using 6-liter and 35-liter cells equipped with the FLSmidth nextSTEP rotor/stator system were studied. The key findings are summarized as follows:

1. In the 6-liter flotation cell, regression analysis revealed that neither J_g nor V_t had a significant effect on the response variables (recovery, grade, and rate constant) at a 95% confidence level. This result suggested that hydrodynamic conditions may have a limited impact on flotation performance in small-scale cells, possibly due to the dominant influence of mineralogical factors. Additionally, the potential overuse of the collector might have overshadowed the effects of J_g and V_t. Future studies should investigate the optimal collector dosage to isolate and better understand the impact of hydrodynamic conditions.
2. In the 35-liter flotation cell, both J_g and V_t significantly influenced the flotation recovery, with J_g exhibiting a negative effect, and V_t a positive impact. Thus, hydrodynamic conditions play a more critical role in flotation performance in larger cells.
3. The observed differences between the 6-liter and 35-liter cells highlighted the importance of scale in flotation; specifically, the difficulties to maintain consistency of all physical and chemical subprocesses at different scales. Therefore, large-scale experiments are crucial for properly evaluating the impact of hydrodynamic conditions in flotation.
4. Particle-based separation modeling using MLA data provided detailed insights into the effect of hydrodynamic conditions at the particle level:
    a. Increasing V_t from 4.2 to 5.5 m/s at a constant J_g of 0.3 cm/s led to improved overall chalcopyrite recovery and a wider concave trend across all particle sizes. This improvement was attributed to enhanced particle-bubble interactions caused by turbulence, mixing, and smaller bubbles.

b. The effect of increasing J_g on chalcopyrite recovery was dependent on V_t. At V_t = 4.2 m/s, increasing J_g slightly improved chalcopyrite recovery, while at V_t = 5.5 m/s, the J_g effect was minor. This behavior was explained by the balance between higher bubble surface area flux and increased detachment forces.

To improve flotation predictions, future research should refine and develop PSMs using data from larger (≥35 liter) machines, incorporating detailed hydrodynamic and mineralogical data. Future work should be focused on the optimization of V_t and J_g in large-scale cells, investigating wider ranges for these variables to improve metallurgical indexes. By implementing these recommendations, further research on this topic will enhance the efficiency and effectiveness of flotation, leading to more sustainable and profitable mineral processing operations.

6 SUMMARY

This thesis investigated the influence of hydrodynamic conditions on the batch flotation performance of a porphyry copper ore. Two flotation scales were studied: 6-liter and 35-liter cells equipped with the FLSmidth nextSTEP rotor/stator system. The main objective was the identification of the effects of variations in impeller tip speed (V_t) and superficial gas velocity (J_g) on performance indices, such as recovery, grade, and rate constant.

Experiments were conducted using a factorial design to evaluate the effects of V_t and J_g on performance parameters. The regression analysis revealed a notable difference in the statistical significance of the studied factors. In the 6-liter cell, neither J_g nor V_t significantly influenced the response variables at a 95% confidence level, suggesting that hydrodynamic conditions may not substantially impact the flotation performance in a small scale. In contrast, the experiments in the 35-liter cell demonstrated significant effects of J_g and V_t on Cu recovery, with J_g exhibiting a negative influence and V_t showing a positive impact. However, for the Cu grade and rate constant, J_g and V_t were not significant factors in the 35-liter flotation tests.

Despite the lack of statistical significance in the 6-liter cell, small-scale machines can still provide valuable insights into the flotation process. To further investigate the flotation performance in the 6-liter cell, representative samples of the flotation products were analyzed by MLA. Particle-based separation modeling (PSM) integrated with MLA data from these tests provided insights into the effect of flotation hydrodynamics on chalcopyrite recovery. Increasing V_t led to improved overall chalcopyrite recovery and a wider concave recovery trend across all particle sizes. The effect of J_g on chalcopyrite recovery depended on V_t. The flotation rate constant varied with particle size, reaching a maximum at around 30 μm. When integrating mineralogical results with PSM, a deeper understanding of mechanisms governing the flotation performance was achieved at the individual particle level (e.g., size-by-size results for liberated chalcopyrite).

The research process faced challenges, such as the limitations of small-scale flotation cells in capturing hydrodynamic effects. These challenges highlighted the need for future research to focus on investigating hydrodynamic parameters in larger flotation cells.

In conclusion, this thesis demonstrated the complex interplay between hydrodynamic factors, particle characteristics, and flotation scale, and their impact on the metallurgical performance of a porphyry copper ore. The findings remarked the importance of considering these factors when designing and optimizing flotation circuits, in scale-up procedures, and when improving the beneficiation of low-grade copper ores.

REFERENCES

Abrahamson, J. (1975). Collision rates of small particles in a vigorously turbulent fluid. *Chemical Engineering Science*, *30*(11), 1371–1379. https://doi.org/10.1016/0009-2509(75)85067-6

Ahmed, N., & Jameson, G. J. (1989). Flotation Kinetics. *Mineral Processing and Extractive Metallurgy Review*, *5*(1–4), 77–99. https://doi.org/10.1080/08827508908952645

Amini, E., Bradshaw, D. J., Finch, J. A., & Brennan, M. (2013). Influence of turbulence kinetic energy on bubble size in different scale flotation cells. *Minerals Engineering*, *45*, 146–150. https://doi.org/10.1016/j.mineng.2013.01.015

Amini, E., Bradshaw, D. J., & Xie, W. (2016). Influence of flotation cell hydrodynamics on the flotation kinetics and scale up, Part 1: Hydrodynamic parameter measurements and ore property determination. *Minerals Engineering*, *99*, 40–51. https://doi.org/10.1016/j.mineng.2016.09.024

Arbiter, N., Harris, C. C., & Yap, R. F. (1976). The air flow number in flotation machine scale-up. *International Journal of Mineral Processing*, *3*(3), 257–280. https://doi.org/10.1016/0301-7516(76)90005-3

Bulatovic, S. M. (2007). *Handbook of flotation reagents: Chemistry, theory and practice. Vol. 1: Flotation of sulphide ores* (Vol. 1). Elsevier.

Christian, R., & Michael, S. (2023). *World Mining Data 2023* (Volume 38; p. 4).

Dai, Z., Fornasiero, D., & Ralston, J. (2000). Particle–bubble collision models—A review. *Advances in Colloid and Interface Science*, *85*(2–3), 231–256. https://doi.org/10.1016/S0001-8686(99)00030-5

Deglon, D. A. (2005). The effect of agitation on the flotation of platinum ores. *Minerals Engineering*, *18*(8), 839–844. https://doi.org/10.1016/j.mineng.2005.01.024

Deglon, D. A., Egya-mensah, D., & Franzidis, J. P. (2000). Review of hydrodynamics and gas dispersion in flotation cells on South African platinum concentrators. *Minerals Engineering*, *13*(3), 235–244. https://doi.org/10.1016/S0892-6875(00)00003-0

Duan, J., Fornasiero, D., & Ralston, J. (2003). Calculation of the flotation rate constant of chalcopyrite particles in an ore. *International Journal of Mineral Processing*, *72*(1–4), 227–237. https://doi.org/10.1016/S0301-7516(03)00101-7

Finch, J. A., & Dobby, G. S. (1991). Column flotation: A selected review. Part I. *International Journal of Mineral Processing*, *33*(1–4), 343–354. https://doi.org/10.1016/0301-7516(91)90062-N

Finch, J. A., Nesset, J. E., & Acuña, C. (2008). Role of frother on bubble production and behaviour in flotation. *Minerals Engineering*, *21*(12–14), 949–957. https://doi.org/10.1016/j.mineng.2008.04.006

Flotation. By A. M. Gaudin. Pp. xv + 552. London: McGraw-Hill Publishing Co., 1932. 36s. (1932). *Journal of the Society of Chemical Industry*, *51*(39), 801–801. https://doi.org/10.1002/jctb.5000513904

Fuerstenau, M. C., Jameson, G. J., & Yoon, R.-H. (Eds.). (2007). *Froth flotation: A century of innovation*. Society for Mining, Metallurgy, and Exploration.

Garcia-Zuniga, H. (1935). The efficiency obtained by flotation is an exponential function of time. *Boln. Soc. Nac. Mineral., Santiago*, *47*, 83–86. Scopus.

Girgin, E. H., Do, S., Gomez, C. O., & Finch, J. A. (2006). Bubble size as a function of impeller speed in a self-aeration laboratory flotation cell. *Minerals Engineering*, *19*(2), 201–203. https://doi.org/10.1016/j.mineng.2005.09.002

Gorain, B. K., Franzidis, J. P., & Manlapig, E. V. (1997). Studies on impeller type, impeller speed and air flow rate in an industrial scale flotation cell. Part 4: Effect of bubble surface area flux on flotation performance. *Minerals Engineering*, *10*(4), 367–379. https://doi.org/10.1016/S0892-6875(97)00014-9

Gorain, B. K., Franzidis, J. P., & Manlapig, E. V. (2000). FLOTATION | Flotation Cell Design: Application of Fundamental Principles. In *Encyclopedia of Separation Science* (pp. 1502–1512). Elsevier. https://doi.org/10.1016/B0-12-226770-2/05781-1

Gorain, B. K., Franzidis, J.-P., & Manlapig, E. V. (1995a). Studies on impeller type, impeller speed and air flow rate in an industrial scale flotation cell — Part 1: Effect on bubble size distribution. *Minerals Engineering*, *8*(6), 615–635. https://doi.org/10.1016/0892-6875(95)00025-L

Gorain, B. K., Franzidis, J.-P., & Manlapig, E. V. (1995b). Studies on impeller type, impeller speed and air flow rate in an industrial scale flotation cell part 2: Effect on gas holdup. *Minerals Engineering*, *8*(12), 1557–1570. https://doi.org/10.1016/0892-6875(95)00118-2

Gorain, B. K., Franzidis, J.-P., & Manlapig, E. V. (1996). Studies on impeller type, impeller speed and air flow rate in an industrial scale flotation cell. Part 3: Effect on superficial gas velocity. *Minerals Engineering*, *9*(6), 639–654. https://doi.org/10.1016/0892-6875(96)00052-0

Gorain, B. K., Franzidis, J.-P., & Manlapig, E. V. (1999). The empirical prediction of bubble surface area flux in mechanical flotation cells from cell design and operating data. *Minerals Engineering*, *12*(3), 309–322. https://doi.org/10.1016/S0892-6875(99)00008-4

Gorain, B. K., Napier-Munn, T. J., Franzidis, J.-P., & Manlapig, E. V. (1998). Studies on impeller type, impeller speed and air flow rate in an industrial scale flotation cell. Part 5: Validation of k-Sb relationship and effect of froth depth. *Minerals Engineering*, *11*(7), 615–626. https://doi.org/10.1016/S0892-6875(98)00046-6

Hassanzadeh, A., Safari, M., Hoang, D. H., Khoshdast, H., Albijanic, B., & Kowalczuk, P. B. (2022). Technological assessments on recent developments in fine and coarse particle flotation systems. *Minerals Engineering*, *180*, 107509. https://doi.org/10.1016/j.mineng.2022.107509

Hu, Y., Qiu, G., & Miller, J. D. (2003). Hydrodynamic interactions between particles in aggregation and flotation. *International Journal of Mineral Processing*, *70*(1–4), 157–170. https://doi.org/10.1016/S0301-7516(03)00023-1

Jameson, G. J. (2012). The effect of surface liberation and particle size on flotation rate constants. *Minerals Engineering*, *36–38*, 132–137. https://doi.org/10.1016/j.mineng.2012.03.011

Kawatra, S. K., & Young, C. (Eds.). (2019). *SME mineral processing & extractive metallurgy handbook*. Society for Mining, Metallurgy & Exploration, Inc.

Lucas, P., Said, B. B., Hassan, A., Rau, F., Hoang, D., & Rudolph, M. (2023). *An open-source laboratory assistant for flotation test work*. Flotation ’23, Cape Town, South Africa.

Mavros, P., & Matis, K. A. (Eds.). (1992). *Innovations in Flotation Technology*. Springer Netherlands. https://doi.org/10.1007/978-94-011-2658-8

Mesa, D., & Brito-Parada, P. R. (2019). Scale-up in froth flotation: A state-of-the-art review. *Separation and Purification Technology*, *210*, 950–962. https://doi.org/10.1016/j.seppur.2018.08.076

Mesa, D., Morrison, A. J., & Brito-Parada, P. R. (2020). The effect of impeller-stator design on bubble size: Implications for froth stability and flotation performance. *Minerals Engineering*, *157*, 106533. https://doi.org/10.1016/j.mineng.2020.106533

Mudd, G. M., & Jowitt, S. M. (2018). Growing Global Copper Resources, Reserves and Production: Discovery Is Not the Only Control on Supply. *Economic Geology*, *113*(6), 1235–1267. https://doi.org/10.5382/econgeo.2018.4590

Nagaraj, D. R. (2005). Reagent selection and optimization—The case for a holistic approach. *Minerals Engineering*, *18*(2), 151–158. https://doi.org/10.1016/j.mineng.2004.10.017

Napier-Munn, T. (2020). *Statistical methods for mineral engineers: How to design experiments and analyse data* (Julius Kruttschnitt Mineral Research Centre, Ed.; Reprinted with corrections and improvements 2020). JKMRC Julius Kruttschnitt Mineral Research Centre.

Nguyen, A., & Schulze, H. J. (2003). *Colloidal Science of Flotation* (0 ed.). CRC Press. https://doi.org/10.1201/9781482276411

Pereira, L., Frenzel, M., Hoang, D. H., Tolosana-Delgado, R., Rudolph, M., & Gutzmer, J. (2021). Computing single-particle flotation kinetics using automated

mineralogy data and machine learning. *Minerals Engineering*, *170*, 107054. https://doi.org/10.1016/j.mineng.2021.107054

Schubert, H. (1999). On the turbulence-controlled microprocesses in flotation machines. *International Journal of Mineral Processing*, *56*(1–4), 257–276. https://doi.org/10.1016/S0301-7516(98)00048-9

Schubert, H., & Bischofberger, C. (1978). On the hydrodynamics of flotation machines. *International Journal of Mineral Processing*, *5*(2), 131–142. https://doi.org/10.1016/0301-7516(78)90010-8

Schuhmann, R. (1942). Flotation Kinetics. I. Methods for steady-state study of flotation problems. *The Journal of Physical Chemistry*, *46*(8), 891–902. https://doi.org/10.1021/j150422a012

Schulze, H. J., & Schulze, H. J. (1984). *Physico-chemical elementary processes in flotation: An analysis from the point of view of colloid science including process engineering considerations*. Elsevier.

Sherrell, I. M. (2004). *Development of a flotation rate equation from first principles under turbulent flow conditions.* [Ph.D. Thesis, Mining and Minerals Engineering, Virginia Polytechnic Institute and State University]. http://hdl. handle.net/10919/29943

Sutherland, K. L. (1948). Physical Chemistry of Flotation. XI. Kinetics of the Flotation Process. *The Journal of Physical and Colloid Chemistry*, *52*(2), 394–425. https://doi.org/10.1021/j150458a013

Tabosa, E., Runge, K., & Holtham, P. (2016). The effect of cell hydrodynamics on flotation performance. *International Journal of Mineral Processing*, *156*, 99–107. https://doi.org/10.1016/j.minpro.2016.05.019

The Role of Critical Minerals in Clean Energy Transitions. (2021). IEA. https://www.iea.org/reports/the-role-of-critical-minerals-in-clean-energy-transitions

Trahar, W. J. (1981). A rational interpretation of the role of particle size in flotation. *International Journal of Mineral Processing*, *8*(4), 289–327. https://doi.org/10.1016/0301-7516(81)90019-3

Valenta, R. K., Kemp, D., Owen, J. R., Corder, G. D., & Lèbre, É. (2019). Re-thinking complex orebodies: Consequences for the future world supply of copper. *Journal of Cleaner Production*, *220*, 816–826. https://doi.org/10.1016/j.jclepro.2019.02.146

Vinnett, L. (2023). A discussion on the limitations of image analysis for determining bubble size in industrial flotation when using algorithms successfully tested from idealized images. *Physicochemical Problems of Mineral Processing*. https://doi.org/10.37190/ppmp/174474

Vinnett, L., Contreras, F., & Yianatos, J. (2012). Gas dispersion pattern in mechanical flotation cells. *Minerals Engineering*, *26*, 80–85. https://doi.org/10.1016/j.mineng.2011.11.003

Vinnett, L., Yianatos, J., & Alvarez, M. (2014). Gas dispersion measurements in mechanical flotation cells: Industrial experience in Chilean concentrators. *Minerals Engineering*, *57*, 12–15. https://doi.org/10.1016/j.mineng.2013.12.006

Wang, D., & Liu, Q. (2021). Hydrodynamics of froth flotation and its effects on fine and ultrafine mineral particle flotation: A literature review. *Minerals Engineering*, *173*, 107220. https://doi.org/10.1016/j.mineng.2021.107220

Wang, H., Yang, W., Yan, X., Wang, L., Wang, Y., & Zhang, H. (2020). Regulation of bubble size in flotation: A review. *Journal of Environmental Chemical Engineering*, *8*(5), 104070. https://doi.org/10.1016/j.jece.2020.104070

Wills, B. A., & Finch, J. E. (2016). *Wills' mineral processing technology: An introduction to the practical aspects of ore treatment and mineral recovery* (Eighth edition). Elsevier.

Yoon, R.-H. (1993). Microbubble flotation. *Minerals Engineering*, *6*(6), 619–630. https://doi.org/10.1016/0892-6875(93)90116-5

Yoon, R.-H. (2000). The role of hydrodynamic and surface forces in bubble–particle interaction. *International Journal of Mineral Processing*, *58*(1–4), 129–143. https://doi.org/10.1016/S0301-7516(99)00071-X

Zhang, W., Nesset, J. E., Rao, R., & Finch, J. A. (2012). Characterizing Frothers through Critical Coalescence Concentration (CCC)95-Hydrophile-Lipophile Balance (HLB) Relationship. *Minerals*, *2*(3), 208–227. https://doi.org/10.3390/min2030208

Appendix 1: Residuals plot for regression analysis of 6-liter flotation test.

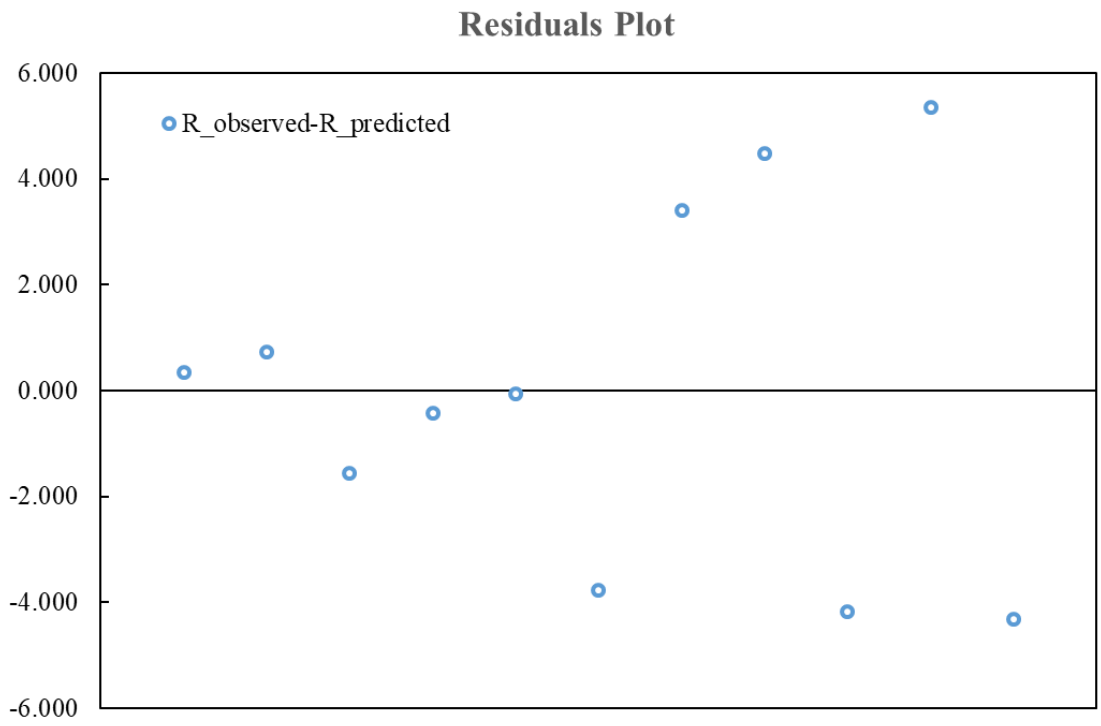

Figure 36. Residuals plot showing the differences between the observed and predicted Cu recovery values. The residuals appear to be randomly dispersed around zero, indicating that the model's assumptions are likely satisfied.

Appendix 2: Results of experimental design of 5 g/t collector dosage

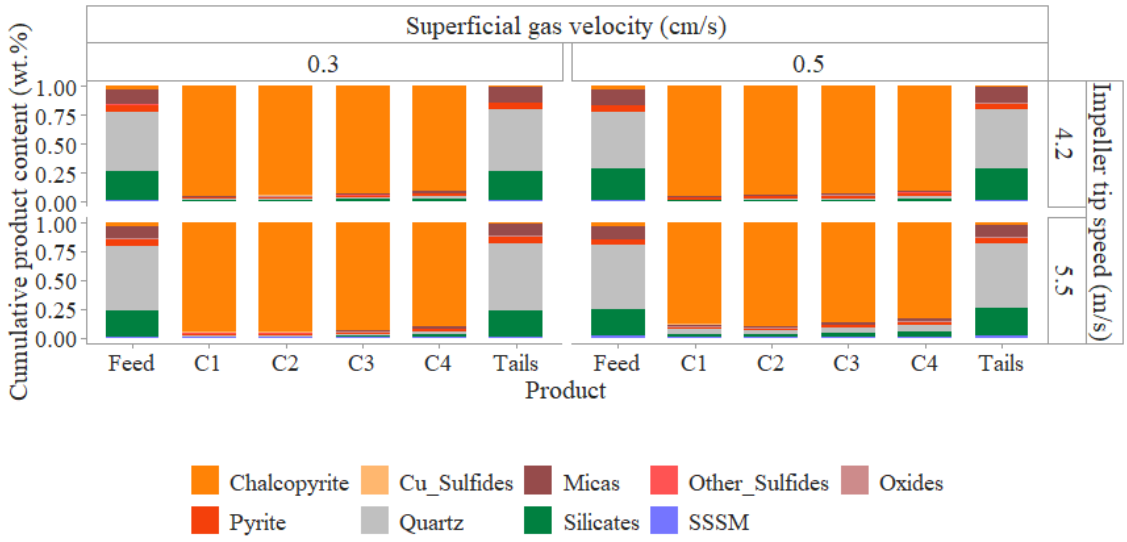

Figure 37. Model mineralogy plot for all tests.

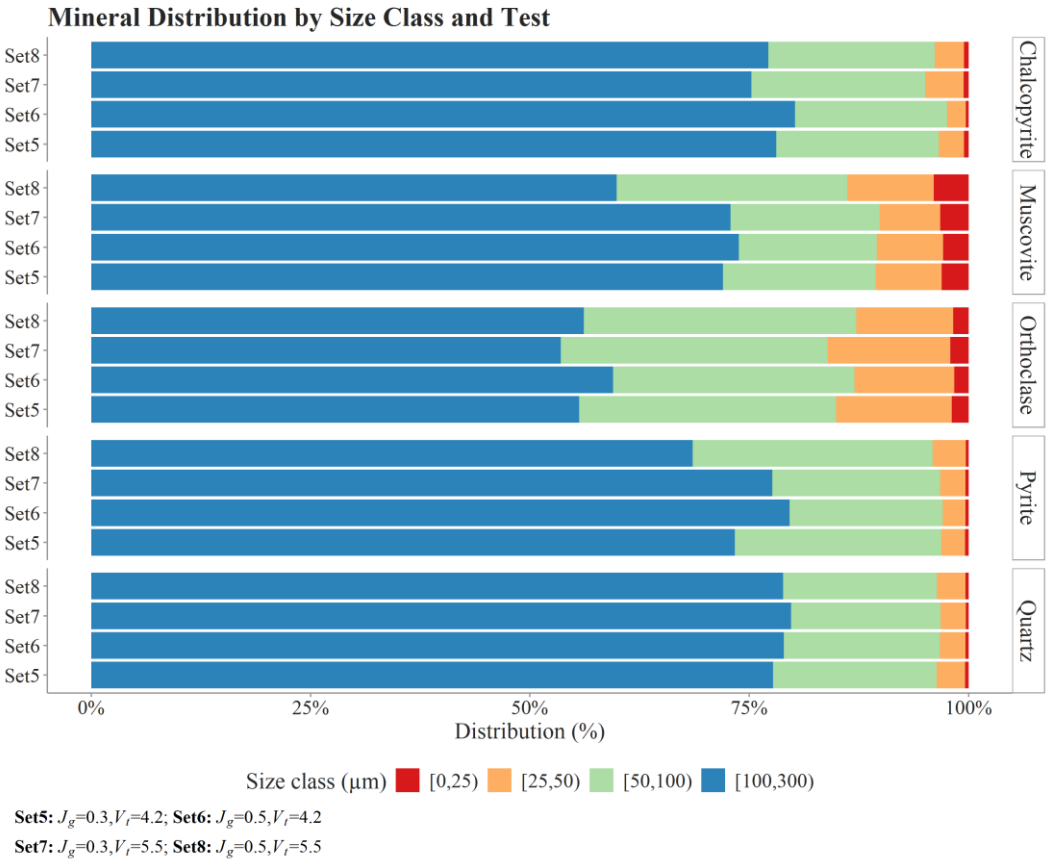

Figure 38. Size-by-composition distribution of the mineral phases in the flotation feed, based on back-calculated data.

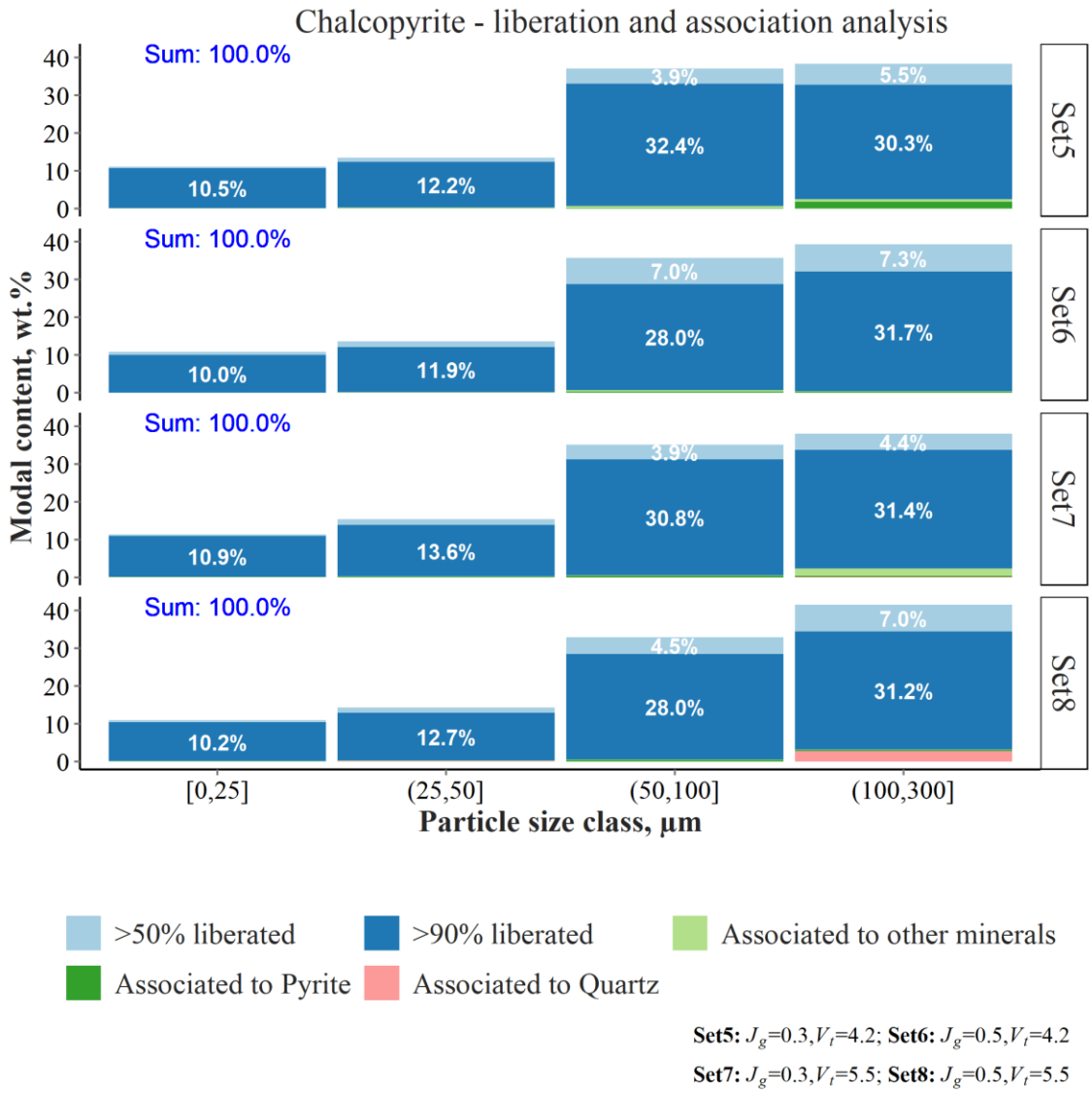

Figure 39. Based on back-calculated feed data, Chalcopyrite liberation and association per size class, showing the mass content.

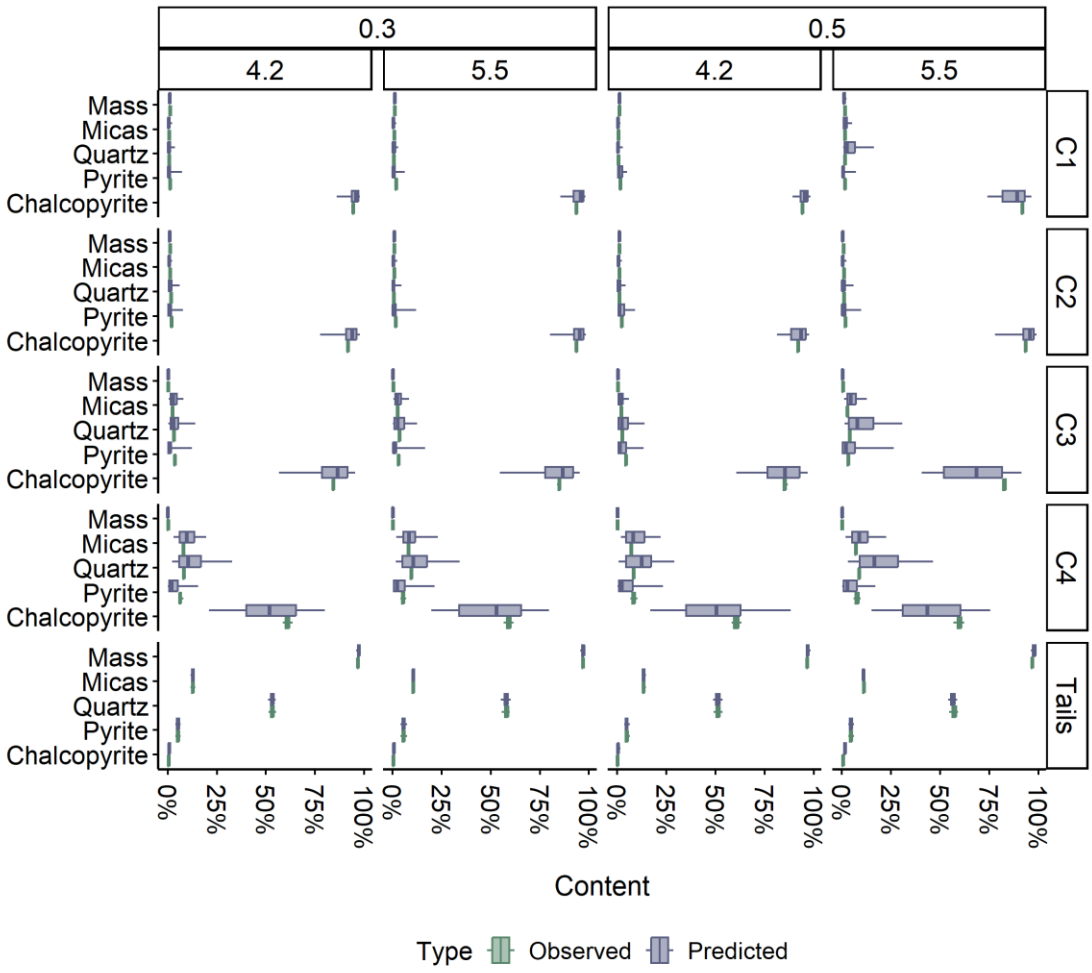

Figure 40. Model errors: predicted vs. observed masses and grades

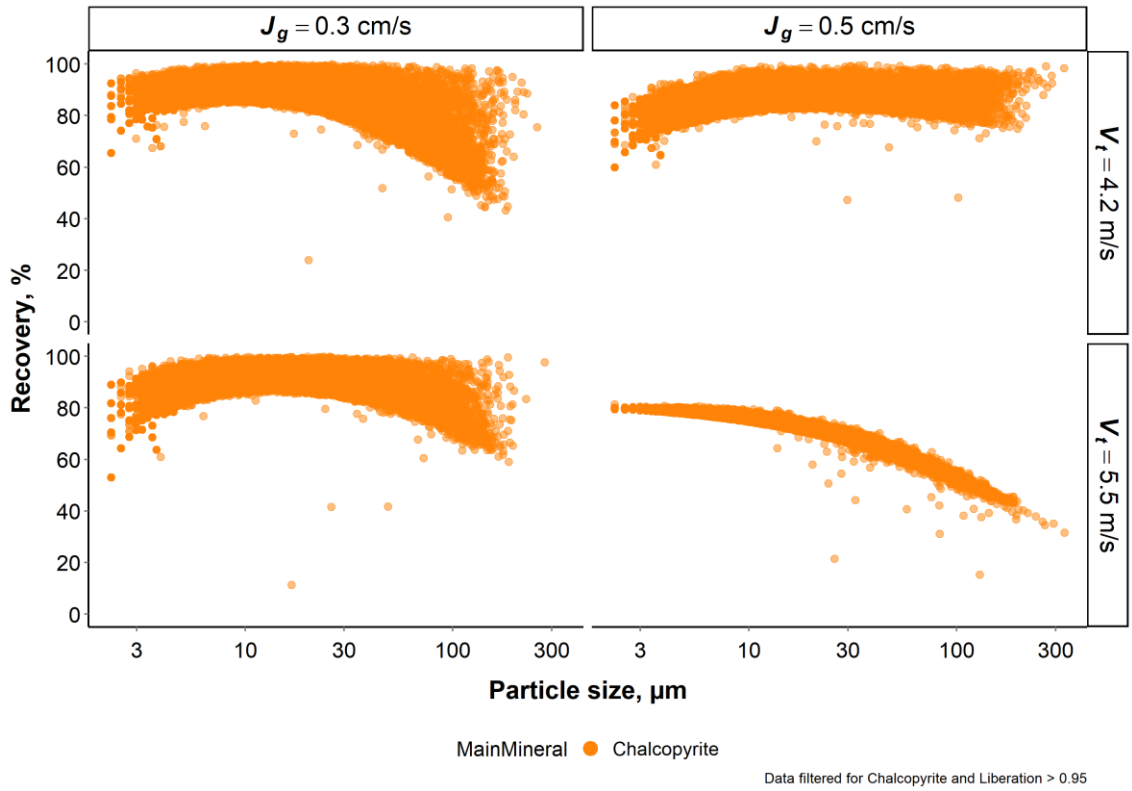

Figure 41. Fully liberated chalcopyrite recovery-particle size relationship under different hydrodynamic conditions.

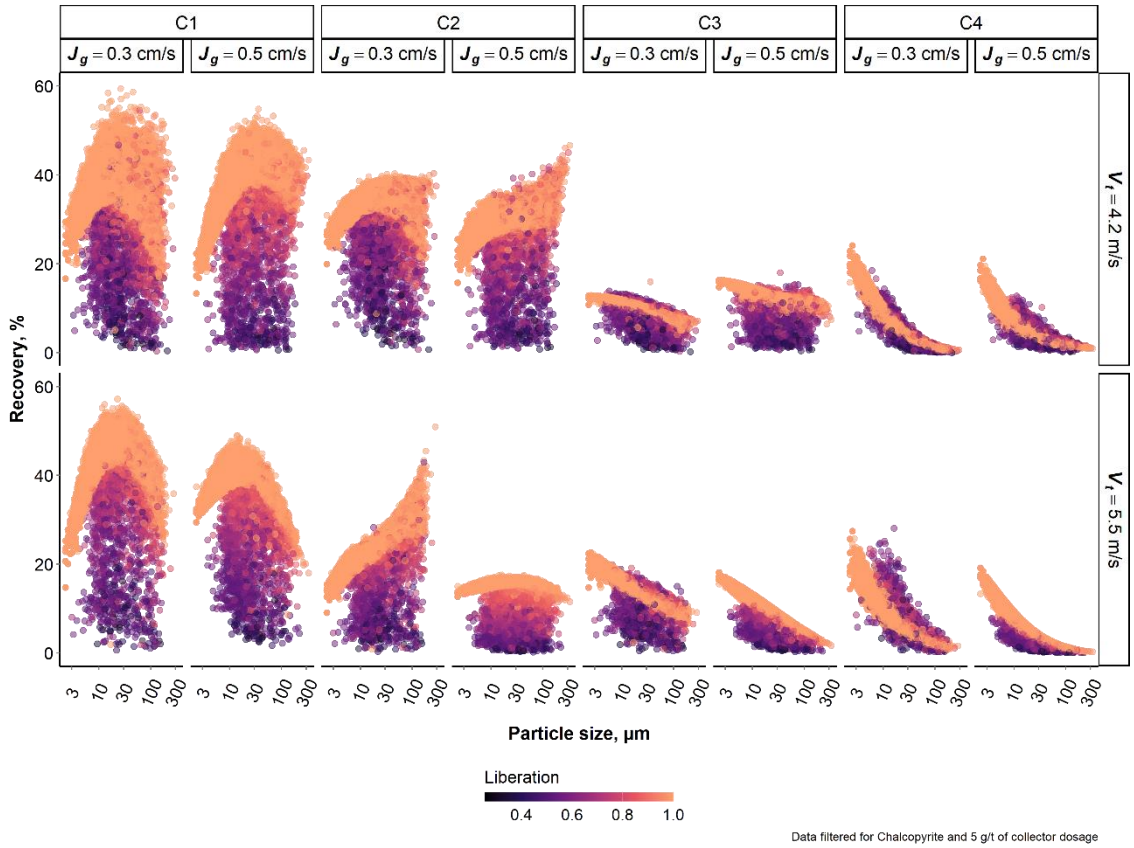

Figure 42. Effect of particle size and liberation degree on chalcopyrite recovery per concentrate under different hydrodynamic conditions.

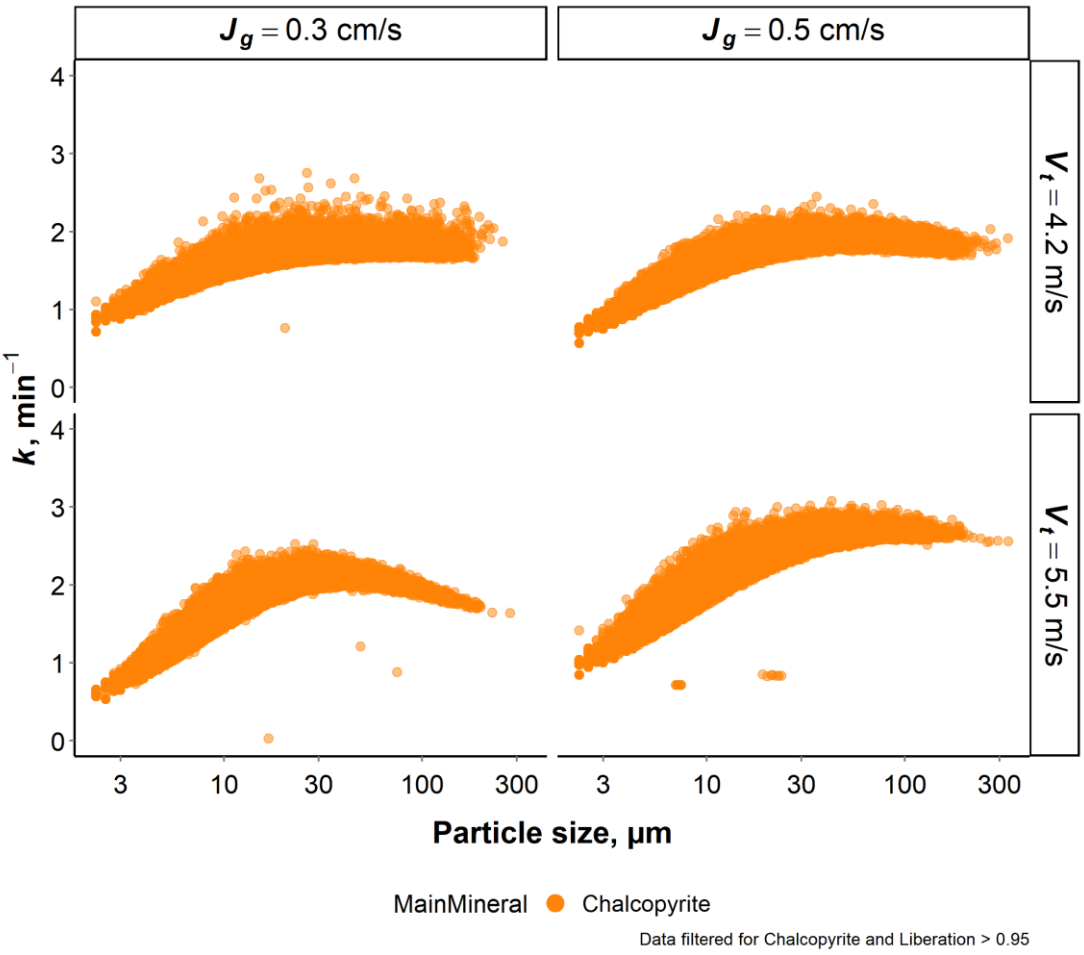

Figure 43. Effect of particle size on the flotation rate constant for the liberated chalcopyrite, at different combinations of J_g and V_t.

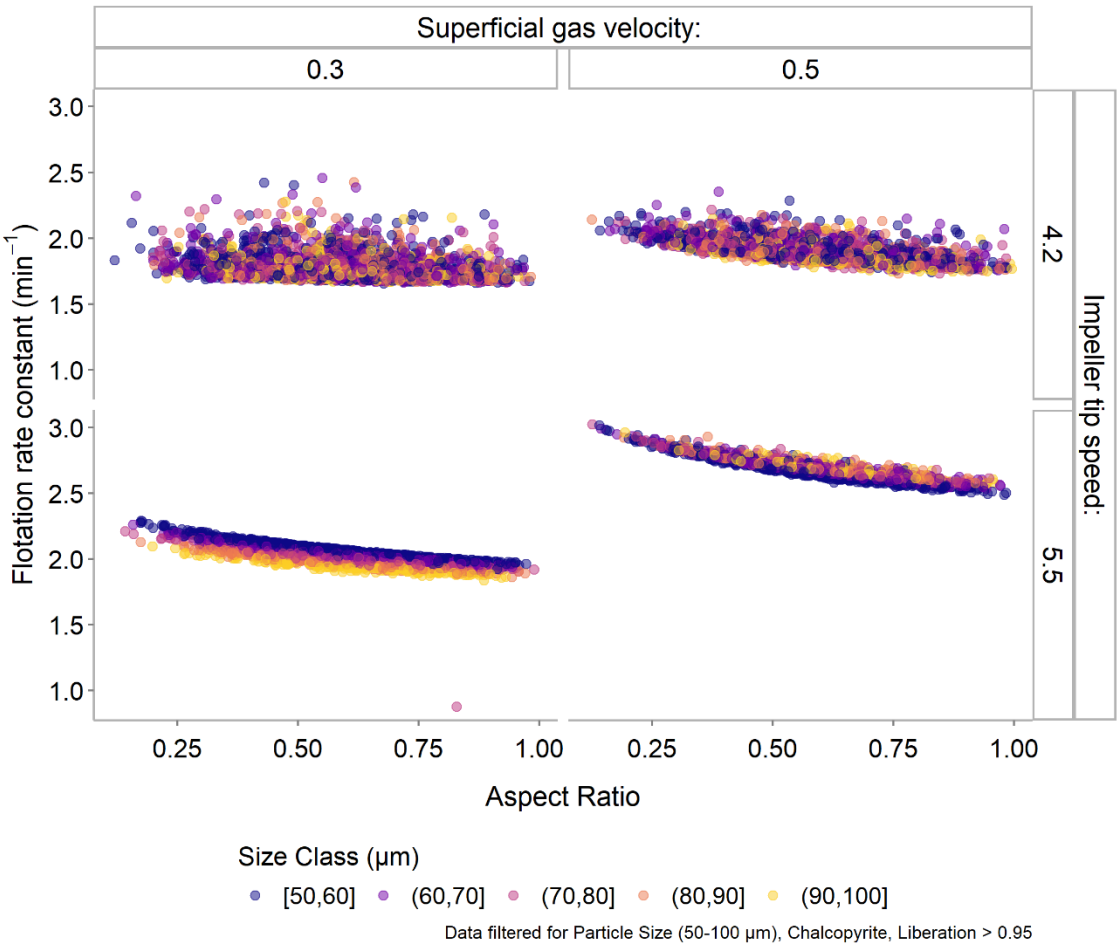

Figure 44. Relationship between the size-by-size recovery and aspect ratio of chalcopyrite particles under different conditions of J_g and V_t. The figure shows the recovery of Cu particles in the 50–100 µm size range across particle aspect ratios from 0.25 to 1.00 under varying V_i and J_9 conditions. The aspect ratio was determined by dividing the minimum Feret diameter by the maximum Feret diameter. The analysis demonstrated that particle recovery remained consistent as the particle aspect ratio increased, suggesting that within the tested range, particle shape had minimal influence on recovery for this size class and displayed a similar trend for other size classes as well. However, it is important to note that these analyses are based on 2D, which may not fully capture the three-dimensional behavior of particles in the samples.